1 **Supplementary Information**

2 Reconciling the total carbon budget for boreal forest wildfire emissions using airborne observations

3

4 Katherine L. Hayden[1]*, Shao-Meng Li[2], John Liggio[1], Michael J. Wheeler[1], Jeremy J.B. Wentzell[1], Amy

5 Leithead[1], Peter Brickell[1], Richard L. Mittermeier[1], Zachary Oldham[1,6], Cris Mihele[1], Ralf M. Staebler[1],

6 Samar G. Moussa[1], Andrea Darlington[1], Mengistu Wolde[3], Daniel Thompson[4], Jack Chen[1], Debora

7 Griffin[1], Ellen Eckert[1], Jenna C. Ditto[5], Megan He[5] and Drew R. Gentner[5]

8 [1]{Air Quality Research Division, Environment Canada, Toronto, ON, Canada}

9 [2]{College of Environmental Sciences and Engineering, Peking University, Beijing, China}

10 [3]{National Research Council of Canada, Ottawa, ON, Canada}

11 [4]{Canadian Forest Service, Natural Resources Canada, Edmonton, ON, Canada}

12 [5]{Yale University, New Haven, CT, USA}

13 [6]{University of Waterloo, Waterloo, ON, Canada}

14

15 *Correspondence to: Katherine Hayden (katherine.hayden@ec.gc.ca)

16

17 **1.0 Methods**

18 **1.1 Aircraft measurements**

19 Table S1 provides a summary of the measurements with associated instrumentation, technical details and

20 related references.

21 **1.1.1 Trace gas measurements**

22 All of the trace gas instrumentation except NH_3 and the CIMS were sampled through PTFE tubing from a

23 main aircraft roof hatch that contained multiple inlet ports through which rear-facing tubing was mounted.

24 The rear-facing inlet minimizes the sampling of particles.

25 **NO, NO$_2$, NO$_y$, SO$_2$** NO and SO_2 were directly measured: NO by chemiluminescence with excess ozone

26 using a 42i TL instrument operated in single mode, while SO_2 was measured by pulsed fluorescence with

27   a 43i TL instrument. A photolytic converter (Air Quality Design Inc.) was used to selectively convert a

28   large fraction of NO_2 to NO. The sum of this NO_2 fraction that was converted to NO plus ambient NO,

29   defined as NO_c, was measured by a second 42i TL chemiluminescent instrument and then NO_2 was

30   calculated based on NO_c, NO and the efficiency of the photolytic converter. NO_y was measured by using

31   an external molybdenum converter heated at 325 °C and placed as close as possible to the sampling point,

32   followed by a third 42i TL instrument. NO and SO_2 calibrations were conducted by generating mixing

33   ratios of 0-100 ppbv using NIST certified cylinders from Scott-Marin (10.3 ppmv accuracy: +/- 2 %), an

34   Environics (Model 6100 Multi-Gas Calibrator), and a Sabio Zero Generator (Model 1001). The

35   efficiencies of the photolytic and NO_y converters were determined using the gas phase titration option of

36   the Environics calibrator. Calibrations were conducted periodically throughout the measurement study

37   using NIST–certified standards. Instrument zeros were performed for these instruments 3-5 times per

38   flight for a duration of ~3-5 minutes each time at the beginning, during and after each flight.

39   **NH_3** Ammonia (NH_3) was sampled through an unfiltered inlet, critical orifice and 4 m of 6.35 mm (¼")

40   outer diameter Sulfinert-coated tubing heated to 90 °C to minimize NH_3 losses to the tubing walls. The

41   flow rate was 2.5 LPM, controlled through a critical orifice near the unfiltered inlet with the pressure in

42   the fluoropel-coated LGR cell being maintained at 100 Torr. For instrument zeros, ambient air was

43   passed through a Teflon filter coated with citric acid. Calibrations were performed using a certified

44   ammonia standard (Air Liquide; 10.0 ppm NH_3 in N_2, accuracy: +/- 5 %), diluted to near-ambient levels.

45   **CO, CO_2, CH_4** CO, CO_2, CH_4 were measured with a Cavity Ring Down (CRD) spectroscopy instrument

46   (Picarro G2401-m).

47   **TC and $NMOG_T$** A second Picarro G2401-m instrument was used to measure total carbon (TC, in units

48   of ppmv C) by passing the sample air through a heated (650 °C) platinum catalyst (Shimadzu), adapted

49   from Stockwell et al. (2018) and Veres et al., (2010) which converted all carbon species to CO_2.

50   Approximately 4 g of platinum catalyst

51   (https://www.elementalmicroanalysis.com/product_details.php?product=B1605&description=High%20Se

52 nsitivity%20Catalyst%20630-00996) was enclosed in a resistively heated ½" O.D. x 12" long stainless

53 steel tube. As the catalyst assembly was mounted on the roof exterior to the aircraft, with no unheated

54 portion of inlet, TC losses were expected to be negligible. $NMOG_T$ mixing ratios in units of ppmv C

55 were quantified by subtracting the ambient CH_4, CO and CO_2 measurements (instrument without the

56 catalyst) from the TC measurements (Fig. S2). Calibrations using two different mixing ratio standards of

57 CO, CO_2 and CH_4, traceable to NOAA GMD standards, were performed for both Picarro instruments

58 during flight (at the beginning and end) to assess instrument drift and sensitivity. No significant drift was

59 observed during each flight. $NMOG_T$ was averaged to 10 sec (from the 2 sec native time resolution) to

60 increase the signal to noise ratio. The uncertainty of each instrument was assessed in flight by

61 overflowing the inlet with a constant flow of calibration gas or an ultra pure nitrogen gas stripped of CO_2

62 via two NaOH pellet traps in series (https://www.sigmaaldrich.com/CA/en/product/supelco/503215). In

63 both cases, this resulted in an uncertainty of approximately 60 ppbv C at the 3σ level for each TC channel

64 (dominated by the precision of the CO_2 measurement) (Fig. S2). These uncertainties were added in

65 quadrature resulting in a 3σ uncertainty of ±85 ppb C for $NMOG_T$. Laboratory experiments indicated that

66 the conversion efficiency of ethane across the catalyst was ~100 %, which is expected to be the most

67 challenging species to combust aside from methane, which is concurrently measured. Additional

68 laboratory experiments using a range of hydrocarbons ($>C_2$) including aromatics also exhibited ~100 %

69 conversion efficiency (Li et al., 2021; Li et al., 2019). The catalyst material was changed after

70 approximately every 5 flights to further ensure minimal changes in efficiency.

71 **CIMS** The CIMS instrument sampled from an insulated rear-facing inlet (PFA, 3/8" OD, ¼" ID) at 7

72 LPM (0°C, 1 atm). The instrument was operated using iodide as a reagent ion. The mass resolution at an

73 internal standard peak ($^{13}CC_2H_6O_2I^-$) was ~5400 Th/Th. The reagent ion was generated by passing 2

74 sLpm (0°C, 1 atm) of UHP N_2 over a methyl iodide permeation tube held at 40 °C. This flow was then

75 passed through a Polonium-210 ionizer (NRD P-2031) into the ion molecule reactor (IMR). A flow of

76 humidified N_2 (20 sccm through a stainless steel bubbler) was also added to the IMR in order to keep the

77 ratio of $I(H_2O)^-/I^-$ as constant as possible. The IMR and small segmented quadrupoles (SSQ) were

78 pressure controlled to 70 and 1.5 mBar respectively using Alicat pressure controllers (PC-EXTSEN).

79 Instrument zeros were performed every 15 min by flooding the inlet with 10 sLpm (0°C, 1 atm) of air that

80 had been passed through a Pt/Pd catalyst (CD Nova) heated to 350 °C followed by bicarbonate and

81 charcoal scrubbers (United Filtration). A flow (50 sccm) of isotopically labelled propanoic acid

82 ($^{13}CC_2H_6O_2$) was constantly added to the inlet during the campaign to track instrument sensitivity.

83 Compounds were identified using known/expected sensitivities and available calibration standards

84 (Tables S3).

85 **PTRMS** The PTR-ToF-MS was operated in a configuration described previously (Table S1). Gases

86 with a proton affinity greater than that of water were protonated in the drift tube. The pressure and

87 temperature of the drift tube region were maintained at a constant 2.15 mbar and 60 °C, respectively for

88 an E/N of 141 Td. The unit contained a catalytic converter heated to 350 °C with a continuous flow of

89 ambient air at a flow rate of one litre per minute. A permeation tube with 1,2,4-trichlorbenzene was

90 placed at the inlet to improve the accuracy of the mass calibration for higher masses. Instrumental

91 backgrounds were performed in flight using a custom-built zero-air generating unit. The data were

92 processed using Tofware software (Tofwerk AG). Calibrations were performed on the ground using gas

93 standard mixtures from Ionicon, Apel-Reimer and Scott-Marrin for 20 compounds (Table S3).

94 Compound identifications for molecular formulas for the PTRMS and CIMS data were assigned based on

95 a limited set of possibilities (particularly for the smaller compounds), known or expected compound

96 sensitivities, and previously published laboratory work by Koss et al. (2018); this is more fully described

97 in the SI Sect. 2.1.3.

98 **AWAS** The Advanced Whole Air Sampler (AWAS) was used to collect ambient samples using 1.33-litre

99 electropolished stainless steel canisters in rack-mounted arrays of 12-canister modules (Lerner et al.,

100 2017, and references therein). A metal bellows compressor (Senior Aerospace Metal Bellows, MB-158)

101 was used to pressurize canisters to approximately 30 PSI over a period of approximately 20 to 30 sec.

102 Sample lines and manifold tubing were continually flushed with ambient air during the flights. Sampling

103   took place by activating module and pump system valving with custom Labview-based software

104   operating a data logger interface (Labjack Corp., Model T7). The samples were analysed between 5 and 9

105   days after the flight with an analytical system installed at the Fort McMurray International Airport. The

106   on-site analytical system consisted of a custom fabricated gas chromatograph (GC) system using

107   cryogenic sample pre-concentration, 2-dimensional gas chromatography, Mass Spectrometric Detection

108   (MS) and Flame Ionization Detection (FID). Sample air was cryogenically trapped at -185 °C on a glass

109   bead-filled trap, thus condensing/solidifying the hydrocarbons, and subsequently thermally desorbing

110   them at 135 °C into the multi-column, multi-oven GC/MS/FID instrument. Trapped sample air volumes

111   were calculated by recording pressure differences in a volume-calibrated downstream vacuum vessel

112   before and after sample trapping. Duplicate analysis was carried out on one canister in each AWAS

113   module. The analytical separation of approximately 120 chemical species was carried out by use of a pre-

114   column (SPB-1) where the initial separation of compounds according to boiling point occurred. The low

115   molecular weight compounds (C_2 to C_4) were then directed to two RTX-QS columns connected in series

116   and quantified by a FID. The higher molecular weight compound stream (C_4 to C_{10}) was subsequently

117   split and simultaneously analysed by a second FID connected to an Aluminum Oxide/KCL column (C_4 to

118   C_8) and by a quadrupole Mass Spectrometer (Agilent Technologies, 5977B) connected to an HP-1 column

119   by means of a fused silica tubing restrictor (C_7 to C_{10}). The precolumn and RTX-QS columns were

120   mounted in the main oven of the gas chromatograph (Agilent Technologies 7890B) and thus were subject

121   to one temperature program. The AlOx/KCL and HP-1 analytical columns were each mounted in a

122   separate temperature-controlled GC oven module (Agilent Technologies, LTM Series II) and operated

123   with a different temperature program. Detector peak areas were calibrated with primary gas standard

124   mixtures in the ppbv concentration range obtained from Apel-Reimer Environmental Inc. (U.S.A.) and

125   the National Physical Laboratory (UK). Compound retention time drift and potential detector sensitivity

126   changes were monitored and compensated for by means of daily analysis of a secondary standard gas.

127   The AWAS modules were cleaned by a custom-fabricated, automated cleaning system similar to that of

128   Lerner et al. (2017).   Toluene, benzene and xylenes were not quantified because the method and

5

129   columns used were not optimized for these compounds. Analytical issues due to incomplete water vapour

130   management in the sample gas stream resulted in retention time shifts and some peak broadening effects

131   resulting in elevated uncertainties. Uncertainties are estimated at ±25 % for C_2 to C_5 and C_6 alkanes

132   detected by FID, and ±40 % for C6 alkenes, and the C_7 to C_{10} species detected by MS.

133   **Cartridges** Integrated gas phase samples were collected using an automated adsorbent tube sampling

134   assembly (i.e. cartridge) that was mounted in an under-wing pod (see Ditto et al., 2021). Adsorbent tubes

135   were packed with quartz wool, glass beads, Tenax TA, and Carbopack X (or "QBTX"), similar to those

136   discussed in Sheu et al. (2018). Samples were shipped to Yale University where offline analysis was

137   conducted using thermal desorption (GERSTEL TD 3.5+) followed by gas chromatography (Agilent

138   7890B), atmospheric pressure chemical ionization, and high-resolution mass spectrometry (Agilent 6550)

139   to speciate gas-phase organic compounds (Ditto et al., 2021, Sheu et al., 2018, Khare et al., 2019). Ion

140   abundances for CH, CHO_1, and CHS_1 species were converted to mass concentrations assuming average

141   response factors that were calculated based on calibrations using the NIST Reference Gulf of Mexico

142   2779 Macondo Crude oil reference material following Khare et al. (2019), which accounts for variations

143   in response and fragmentation between components of the complex mixture. CHN_1 species were not

144   quantitatively converted to mass due to the lack of comprehensive and available authentic standards. The

145   reported emissions are subject to potential variations in sampling efficiency within the under-wing

146   sampling pod across C_{10}-C_{25} and, in the event of losses due to analyte breakthrough, would likely be

147   considered lower limit estimates. Prior breakthrough testing with QBTX adsorbent tubes and similar

148   sampling conditions to those used in this study showed that analyte trapping efficiency in the same carbon

149   number range was generally greater than 85 % (Sheu et al., 2018). For CH, CHO_1, and CHS_1, each group

150   of isomers at a given carbon number was categorized by molecular formula, according to their double

151   bond equivalents (DBE) ranging from 0 to 15. Emission ratios (to in-plume CO) were estimated for CH,

152   CHO_1 and CHS_1 using observed concentrations for the C_{10}-C_{25} species summed across DBEs. Further

153   discussion of these methods can be found in Ditto et al. (2021), including in the SI (i.e., Section S3).

1.1.2 Particle measurements

Particles were sampled from a forward-facing isokinetic stainless steel diffuser inlet (Droplet Measurement Technologies) that was positioned near the top of the fuselage forward of the engine on the starboard side. Theoretical calculations that take into account the inlet dimensions, volume flow and velocity indicated a 97 % transmission efficiency for particles < 1 µm through the inlet. Air was pulled through the inlet into a main 0.5" O.D. stainless steel sampling line maintained at the isokinetic rate of 70 LPM by two venturis mounted on the fuselage in the aft section of the aircraft. The aerosol instruments subsampled from the main sampling line.

AMS The high resolution aerosol mass spectrometer (AMS) (Aerodyne) measures submicron particles that are sampled through a critical orifice and focussed through an aerodynamic lens into a region of low vacuum. The particles impact a heated surface (600 °C), are vapourized and ionized by 70eV impaction. Ions are then transferred to a time-of-flight mass spectrometer (Tofwerk) where they are accelerated by electric fields and separated by their velocities which are dependent on their mass to charge ratios. Ions are then detected by charged microchannel plates. The AMS was operated only in V mode with 10 sec time resolution. Several ionization efficiency calibrations performed prior to and during the field campaign varied by <10 %. To determine the AMS collection efficiency, number concentrations measured by an Ultra High Sensitivity Aerosol Spectrometer (UHSAS; Droplet Measurement Technologies Inc.) over a size range of 60 nm to 1 µm were converted to volume concentrations using mid-point bin diameters and assuming spherical shapes. Total mass was calculated from the UHSAS measurements based on the composition-weighted proportional density determined from the AMS. A collection efficiency of 0.5 was determined. Detailed investigations and discussions around the collection efficiency of the AMS can be found in the literature (Middlebrook et al., 2012; Dunlea et al., 2009; Kleinman et al., 2008; Drewnick et al., 2004; Quinn et al., 2006). PM_1 is the sum of the mass concentrations of AMS components (OA, NO_3, SO_4 and NH_4). The PM_1 from this study is compared with the $PM_{2.5}$ EF from the Andreae (2019) literature review of boreal forest wildfire studies. While these

179   measurements represent PM over different size ranges ($< 1\mu m$ vs $<2.5\mu m$), the difference is not expected

180   to be significant based on typical size distributions of wildfire emissions (Andreae 2019; Reid and Hobbs,

181   1998; Reid et al., 2005). This approach has been used previously in literature reviews of EFs for wildfire

182   emissions (Andreae 2019; Akagi et al., 2011).

183   **BC** The SP2 measures the mass of rBC contained in individual aerosols through the laser-induced

184   incandescence of heated rBC-containing aerosols (Stephens et al., 2003; Baumgardner et al., 2004;

185   Schwarz et al., 2006). The SP2 was calibrated using fullerene soot (Alpha Aesar lot# F12S011) (Moteki

186   and Kondo, 2010; Kondo et al., 2011; Laborde et al., 2012) nebulized from a water suspension and passed

187   through an aerosol particle mass analyzer (Kanomax APM3600) to select particles with masses ranging

188   from 0.2 fg/particle to 48 fg/particle. Extremely large particles containing more than 520 fg of rBC were

189   excluded from analysis due to saturation of the detector (these accounted for only 2×10^{-3} % of the total

190   number of rBC containing particles measured by the SP2).

191   **UHSAS** Particle size distributions were measured using an Ultra-High Sensitivity Aerosol Spectrometer.

192   The UHSAS measures the size of individual aerosols passing through a laser beam via Mie scattering (Cai

193   et al., 2008; Kupc et al., 2018). These particles are classified into 99 log-normally spaced bins across the

194   measurement range. Periods where the particle concentration measured by the UHSAS exceeded 3000

195   particles s^{-1} were excluded from this analysis due to the potential of coincident particles passing through

196   the laser beam. The UHSAS particle sizing was verified using NIST traceable polystyrene latex (PSL)

197   nanospheres of multiple sizes across the measurement range. Total particle mass was calculated from the

198   UHSAS measurements assuming a density of 1.2 g cm^{-3}, based on the composition-weighted proportional

199   density determined from the AMS.

200   **1.1.3 Identification of organic compounds**

201   Three methods were used to provide detailed measurements of gas-phase organic compounds that

202   included the PTRMS, CIMS, and canister samples (AWAS). The PTRMS and CIMS are able to resolve

203   the molecular formula of isobaric species, but cannot distinguish isomers, while the AWAS system can

204   identify and speciate individual compounds. For the PTRMS measurements, compound molecular

205   formulae were assigned based on a limited set of possibilities (particularly for the smaller compounds),

206   known or expected compound sensitivities, and comparing with previously published laboratory work by

207   Koss et al. (2018) based on typical NMOG structures observed in biomass burning emissions. Koss et al.

208   (2018) used a combination of gas-chromatography (GC) pre-separation, NO^+ CIMS and time series

209   correlations to identify 156 compounds measured in biomass burning laboratory experiments with a

210   PTRMS. Additional comparisons were made with PTRMS ion masses reported in Permar et al. (2021)

211   where they used a PTRMS with two GC methods to speciate isomers for some PTRMS ion masses. For

212   formulas with multiple isomer contributions that were not speciated by the PTRMS, or provided by the

213   AWAS, the fractional contributions in Koss et al. (2018) and Permar et al. (2021) were used to identify

214   the dominant ion and/or contributing compounds. Although the Koss et al. (2018) work was based on

215   laboratory measurements, Permar et al. (2021) found that isomer contributions did not vary much between

216   24 fires types across the WE-CAN airborne field campaign in western US, which were mainly dominated

217   by fires of pine, fir and spruce trees. For example, in Koss et al. (2018), for the mass spectral ion of

218   C_3H_6O (m/z 58.08), the contribution from acetone was set at 100 % and propanal 0 %, only slightly

219   different from the contribution of 83±6 % for acetone determined by Permar et al., 2021; thus this

220   compound was identified as acetone in this work. Another example is C_4H_8O at m/z 70.091 that has

221   potential contributions from methyl vinyl ketone (MVK), methacrolein and crotonaldehyde, both Koss et

222   al. (2018) and Permar et al. (2021) both reported that MVK is the largest contributor at 48 % and 60±9 %

223   respectively; the compound was labelled here as all three. For C_8H_{10} (m/z 106.168), there are

224   contributions from ethylbenzene, m- and p-xylenes and o-xylene identified as 10%, 68% and 23%,

225   respectively (Koss et al., 2018), with slightly different isomer contributions as per Permar et al. (2021).

226   In this study, as it was not possible to speciate C_8H_{10} with the AWAS system, it is simply identified as C8

227   aromatics. Similarly, $C_{10}H_{16}$, (m/z 136.238) is identified as total monoterpenes in the present study, with

228   expected contributions from multiple species including alpha and beta pinene, camphene, myrcene, and

229   tricyclene (Permar et al., 2021; Hatch et al., 2017). C_5H_8 at m/z 68.119 was identified as isoprene in the

230 present study, recognizing that there may be a fractional contribution to this mass from methyl-3-buten-2-

231 ol (MBO), although Permar et al. (2021), suggests that MBO may not be significant, based on their

232 analysis of western US wildfires.

233   For the CIMS, the iodide reagent ion chemistry is most sensitive to polar compounds, particularly

234 carboxylic acids and less sensitive to non-polar compounds (Table S1). Compounds were identified using

235 these known/expected sensitivities and available calibration standards. The AWAS provided speciated

236 measurements of hydrocarbons ($\leq$C10), and no oxygenates.

237

238 **1.1.4 Overlapping compounds** There were a number of compounds (or molecular formulae) that were

239 measured by both the PTRMS and the AWAS, as well as compounds that overlapped between the

240 PTRMS and CIMS. Tables S4 and S5 summarize the decisions of overlapping compounds that were

241 retained for derivation of EFs and ERs, as well as for the carbon/nitrogen budget analyses. For the

242 PTRMS and AWAS, for some molecular formulae, the AWAS provided measurements of individual

243 isomers, while the corresponding PTRMS measurement was expected to reflect the sum of multiple

244 isomers. Comparisons between these two methods are challenging due to the influence of isomers in the

245 PTRMS signal, and the fact that a number of the PTRMS compounds are determined using calculated

246 sensitivities (i.e. not directly calibrated with a standard) with estimated uncertainties of 50 %. These

247 factors limit a comparison between the AWAS and PTRMS for isoprene (C_5H_8) which is shown in Fig.

248 S3a. The comparison for Screens 1 through 3 shows good agreement with an r_2=0.87. When including

249 only Screen 1 data, there are two data points (in the SP) where the PTRMS is a factor of 2.5 to 3 higher

250 than the AWAS, resulting in a lower r^2=0.45. Although the PTRMS isoprene signal is known to have

251 interferences from cycloalkanes, these compounds are not expected to be emitted from wildfires. 2-

252 methyl-3-buten-2-ol (MBO) produces a fragment at m/z 69.070 that is not separated in the PTRMS, and

253 can also interfere with the isoprene measurement. We do not have measurements to confirm the impact

254 of MBO on the isoprene signal. However, Permar et al. (2021) reported that PTRMS derived isoprene

255 measurements during their study were approximately 2x higher than the AWAS isoprene while sampling

256   smoke, but MBO which was measured during that study was considered too low to account for the higher

257   than expected isoprene. In the present study, it is possible that there were contributions from other

258   unknown isomers to the PTRMS signal in the fresh smoke plumes along Screen 1. Due to these

259   uncertainties, and the comparatively fewer in-plume AWAS samples, EFs and ERs for isoprene are

260   reported from both the PTRMS and AWAS, and isoprene from the PTRMS was used in the carbon

261   budget (Table S4).

262   In deriving EFs and ERs, both the PTRMS and AWAS measurements were included to retain as

263   much information as possible. To avoid double-counting compounds in the carbon and nitrogen budget

264   analyses, only the PTRMS measurement was typically included as it is expected to reflect a sum of

265   multiple isomers, thus, accounting for more carbon. For example, at the molecular formulas of C_5H_{10}, the

266   PTRMS measurements are expected to reflect the sum of all the isomers, whereas 7 compounds were

267   speciated from the AWAS i.e. c-2-pentene, cyclopentane, 1-pentene, 2-me-1-butene, 3-methyl-1-butene,

268   t-2 pentene, and 2-me-2-butene. In this case, EFs and ERs were derived for both the PTRMS and AWAS

269   measurements, but only the PTRMS measurements were included in the budget analyses.

270   Between the PTRMS and CIMS, there were 18 overlapping molecular formulae. Although

271   comparisons of exact masses between the PTRMS and CIMS are complicated because of the influence of

272   isomers in the PTRMS signal, four exact masses were identified as the same compound including acetic

273   acid, acrylic acid, formic acid, and isocyanic acid. Figure S3 shows a comparison for the first three

274   compounds, but excludes isocyanic acid as this compound can hydrolyze in the PTRMS drift tube. The

275   CIMS provided measurements of pyruvic acid, but the PTRMS signal at the same mass is likely affected

276   by inlet line losses. Acetic acid and acrylic acid show good agreement with $r^2 > 0.8$ with the PTRMS in-

277   plume measurements ~20 % higher than the CIMS (Fig. S3a, b); this is likely due to additional

278   contributions to the PTRMS signal at these respective exact masses. The comparison for formic acid

279   (Fig. S3c) is poor ($r^2 = 0.3$) likely because the PTRMS measurements are noisy and have a high detection

280   limit of 2 ppbv, whereas the CIMS detection limit is 0.097 ppbv. The CIMS measurements were also

281   directly calibrated (Table S2), whereas the PTRMS formic acid sensitivity (and other compounds) were

282   calculated, and as such, the CIMS measurements for the overlapping compounds were retained for

283   analysis (Table S5). . The remaining overlapping formulae between the CIMS and PTRMS were

284   calibrated with different analytes, and thus assumed to be different species. While there may in fact be

285   some overlap between isomers contributing to these formulae, their overall contribution to the TC budget

286   is small (<4 %). An attempt was made to quantify as many other peaks that were present in the CIMS

287   mass spectra as possible and apply sensitivity factors. However, the available sensitivity factors were

288   based on laboratory experiments investigating anthropogenic emissions and highly uncertain for biomass

289   burning measurements. Nevertheless, application of these sensitivity factors resulted in average mass

290   from the CIMS spectra totalling < 1.5 % of the TC, so although uncertain, exclusion of these masses is

291   not expected to significantly influence the total carbon budget. It is assumed that all the acids measured

292   by the CIMS are non-aromatic for classifying into chemical structural categories.

293

294   **1.2 Mass balance method for estimating aircraft-derived emission rates**

295   The Topdown Emission Rate Retrieval Algorithm (TERRA) was designed to estimate emission rates of

296   pollutants measured by aircraft. The algorithm is based on the Divergence Theorem to achieve mass

297   balance and been extensively applied to a range of pollutants measured by aircraft (e.g. Hayden et al.,

298   2021; Baray et al., 2018; Li et al., 2017; Liggio et al., 2017; Gordon et al., 2015). An extension of

299   TERRA previously used for estimating pollutant mass transfer rates across virtual aircraft screens (e.g.

300   Hayden et al., 2021; Baray et al., 2018) was used in the present study to estimate emission rates of NO_x,

301   CO, PM_1 and NH_3 using Screen 1 data. Briefly, pollutant concentrations and horizontal wind speeds were

302   mapped to virtual screens and interpolated using a kriging function, as well as extrapolating the

303   measurements from the lowest aircraft altitude to the surface using applicable extrapolation profiles.

304   Mass transfer rates were derived by integration of the horizontal fluxes across the plume on the screen in

305   units of t h^{-1}. The main uncertainty in the mass transfer rate is due to extrapolation to the surface as

306   described previously (e.g. Gordon et al., 2015 and Hayden et al., 2021).

307

2.0 Flight and fire description

309   The 18BN-Larry fire (the Lac LaLoche fires) was detected by the Saskatchewan wildfire

310   management agency on June 23, 2018. Satellite images showed fire hot spots on June 23 and by the

311   evening of June 23 it grew to 1,250 hectares (ha) and to 2,600 ha on June 24th. On the morning of June

312   25, 2018, there was a very weak nocturnal inversion and moderately strong south to southeast winds at 33

313   knots above the inversion. The range of fire intensities during the previous night, as well as the observed

314   high humidity (80-90 %) and light to moderate winds observed at the surface also indicates that the fire

315   source at the time of aircraft sampling was in a smoldering combustion state. Flight tracks were flown at

316   Lagrangian distances downwind of the wildfire. Multiple passes (i.e. transects) perpendicular to the

317   plume direction were made at different altitudes. Two plumes were identified: the SP was clearly due to

318   the fire hot spots identified by MODIS (green dots encompassed by a polygon), but the source of the NP

319   is less certain. It is possible that MODIS was unable to detect the fire source because the fire heat

320   signature was below the threshold for satellite instrument detection. However, surface wind

321   measurements at Lac LaLoche (SI Table S1 in McLagan et al., 2021) show that the wind direction was

322   southerly just prior (approx. 30 min) to the start of the aircraft measurements, and then shifted to

323   southeast (135+/-13°) for the duration of the aircraft flight. Therefore, it is likely that the NP was from

324   the same fire source as the SP that had been transported in a northerly direction just prior to aircraft

325   sampling, and subsequently moved to a northwesterly direction with the wind change. The width of the

326   SP and NP was approximately 14-37 km separated by approximately 8-19 km depending on the sampling

327   altitude, and with an aircraft speed of ~90 m s^{-1}, the plumes were traversed in 3-7 min (Fig. 2).

328

329

3.0 Combustion state

331   The combustion efficiency (CE) can be used to characterize and compare the combustion state of

332   the fire, (i.e. the fraction of fuel carbon converted to atmospheric CO_2) (Ward and Radke, 1993). The CE

333   is dependent upon many factors including fire combustion state, fuel chemistry, fuel geometry, growth

334   stage, moisture content and meteorological conditions such as wind speed and temperature. In a flaming

335   fire, high temperature reactions tend to go to completion (>90 %) as rapid reaction of O_2 with the fuel C,

336   H, N and S produces highly oxidized gases including CO_2, NO_x, and SO_2 and BC. As a fire progresses,

337   incomplete combustion characteristics of smoldering fires becomes more dominant resulting in a larger

338   proportion of the emitted carbon in the form of CO, CH_4, NMOC, and OA. Airborne measurements tend

339   to sample a mixture of combustion states; however, there tends to be a dominant phase of combustion at

340   different fire stages (Andreae and Merlet, 2001). If only accounting for CO_2 and CO, the MCE for the SP

341   is 0.90±0.01 and NP is 0.88±0.01, higher than the CE by 7.1 % and 6.6 % for the SP and NP,

342   respectively. These differences are driven mostly by the additional contribution from NMOGs indicating

343   the importance of their inclusion in assessing fire combustion state.

344   Since the flaming phase was likely more than 14 hrs prior to aircraft sampling, it is possible that

345   the emissions from this fire may also reflect a residual smoldering combustion (RSC) component. RSC

346   produces emissions from combustion of forest floor and woody debris that are not associated with

347   flaming, can be sustained for long periods of time after the passage of a flame front, and are not strongly

348   lofted through fire-induced convection (Bertschi et al., 2003). It is noted though that observations of

349   increased levels of flaming compounds in the plumes including CO_2 and BC (Fig. S4) suggest that to

350   some extent, flaming processes also contributed to the release of these compounds. It is likely that

351   different parts of the fire had varying mixtures of smoldering, flaming and residual combustion processes,

352   but the evidence strongly suggests that the Lac LaLoche fire was predominantly in a smoldering

353   combustion state during the aircraft measurement time period. Smoldering fires can create persistent and

354   poorly ventilated smoke that can be a significant driver in remote community evacuations (McGee, 2020).

355   In addition, boreal fires in this region tend to exhibit a large component of smoldering combustion which

356   can consume large amounts of above and below ground biomass (Akagi et al., 2011).

357 Table S1. Measurements with associated instrument, principle of operation, sampling time resolution,
358 uncertainty, detection limit, and applicable method references.

Measurement	Instrument	Principle of measurement	Time Resolution (sec)	Uncertainty	Detection Limit	Reference
NO	Thermo 42i	Chemiluminescence with O_3	1	±5 %	3σ at 1 sec 0.17 ppbv	Clyne at al., 1964 Ridley et al., 1990
NO_2	Thermo 42i	Photolysis + chemiluminescence with O_3	1	±7 %	3σ at 1 sec 0.43 ppbv	Penkett et al., 2011
NO_y	Thermo 42i	Heated (350°C) and molybdenum catalyzed conversion + chemiluminescence with O_3	1	±5 %	3σ at 1 sec 0.18 ppbv	Fehsenfeld et al., 1987; Williams et al., 1998
SO_2	Thermo 43i	UV pulsed fluorescence	1	±5 %	3σ at 1 sec 1.25 ppbv	Stecher et al., 1997
O_3	Thermo 42i	Chemiluminescence	1	±5 %	3σ at 1 sec 0.52 ppbv	N/A
NH_3	LGR model 911-0039	Absorption	1	±5 %	2.1 ppbv at 1 sec 0.3 ppbv at 60 sec	Leifer et al., 2017
Hg (GEM)	Tekran 237X	Fluorescence	120	±0.054 ng m^{-3}	<0.1 ng m^{-3}	Cole et al., 2014; McLagan et al., 2021
CO, CO_2, CH_4	Picarro G-2401-m	Cavity ring down spectrometry	2	CH_4 ~±3 ppbv	N/A	Baray et al., 2018
Total Carbon (TC)	Picarro G-2401-m	Heated (650°C) platinum catalyzed conversion to CO_2	2	3σ at 10 sec ±60 ppbv	N/A	Stockwell et al., 2018; Veres et al., 2010.
Total non-methane organic gases ($NMOG_T$)	Picarro G-2401-m x 2	Difference method, heated (650°C) platinum catalyzed conversion to CO_2	10	3σ at 10 sec ±85 ppbv	85 ppbv 3σ at 10 sec	Stockwell et al., 2018; Veres et al., 2010
VOCs	CIMS	Chemical ionization/mass spectrometry	1	±10-50% compound dependent	See Table S2	Liggio et al., 2017; Lee et al., 2014
VOCs (≤C10)	AWAS	Grab samples/GC with MS and FID analysis	20-30	<C6 ±25% ≥C_6 ±40%	0.7 to 12.9 pptv for compounds from C_2 to C_8; 1 to 242 pptv for C_9 and C_{10} compounds	N/A
VOCs	PTRMS	Proton transfer/ionization/mass spectrometry	1	VOCs with available standards: ±15% except CH_2O at±20%; Calculated	Range of 0.005 to 1 ppbv, CH_2O 4.6 ppbv at 1 sec	Li et al., 2017; Sekimoto et al., 2017

				VOCs: ±50%		
VOCs-SVOCs (C10-C25)	Custom packed adsorbent tubes	Offline analysis with TD-GC-APCI-Q-ToF	Variable (245-3140 sec per tube)		1 ppt	Sheu et al., 2018; Khare et al., 2019; Ditto et al., 2021
Particle chemical composition	Aerosol mass spectrometer	Volatilization, ionization and mass spectrometry	10	OA: ±35% SO_4: ±25% NO_3: ±20% NH_4: ±25%	OA:0.24 µg m^{-3} SO_4: 0.05 µg m^{-3} NO_3: 0.035 µg m^{-3} NH_4: 0.15 µg m^{-3} at 10 sec	DeCarlo et al., 2008; Jimenez et al., 2003; Allan et al., 2003
Black carbon	SP2	Incandescence	1	15 %	0.01 µg m^{-3} at 1 sec	Stephens et al., 2003; Baumgardner et al., 2004; Schwarz et al., 2006
Particle size distributions (60 -1000 nm)	Ultra-High Sensitivity Aerosol Spectrometer (UHSAS)	Particle light scattering	1	10 %		Cai et al., 2008; Kupc et al., 2018

359

360
361

362

363

364

365

366

367

368

369

370

371

372

373

374

375

376 Table S2. Standards used to calibrate the CIMS, as well as the compound uncertainty, detection limit and
377 applicable method reference. The iodide chemistry is most sensitive to polar compounds and less
378 sensitive to non-polar compounds. The sensitivity tends to increase for keto-, hydroxy- and acid groups,
379 in order. Most of the keto- groups are attached to a carboxylic acid. For the larger acids (>C4) where there
380 can be several isomers, they are generally identified as saturated C4 carboxylic acids and unsaturated C5
381 acids.

Molecular weight	Molecular formula	Compound Name	Calibration standard	Calibration Source	Uncertainty (%)	Detection Limit (pptv)	Reference
27.026	HCN	hydrogen cyanide	Hydrogen Cyanide	High Pressure Cylinder (Air Liquide)	20	17	Stockwell et al 2018
32.06	SO_2	sulphur dioxide	Sulfur Dioxide	High Pressure Cylinder (Air Liquide)	N/A	N/A	Lee et al 2018
43.025	HNCO	isocyanic acid	Isocyanic Acid	Thermal Decomposition/ Diffusion	30	10	Roberts et al 2010
46.025	CH_2O_2	formic acid	Formic Acid	Liquid Standard supplied by Liquid Calibration Unit (LCU)	20	156	Mungall et al 2017
47.013	HONO	nitrous acid	Nitrous Acid	Acid Displacement (output quantified by ion chromatography)	30	12	Roberts et al 2010
57.052	C_2H_3NO	hydroxy acetonitrile	Glycolic Acid Nitrile	Liquid Standard supplied by Liquid Calibration Unit (LCU)	20	0.12	Mungall et al 2017
60.052	$C_2H_4O_2$	acetic acid	Acetic Acid	Liquid Standard supplied by Liquid Calibration Unit (LCU)	20	576	Mungall et al 2017
63.012	HNO_3	nitric acid	Nitric Acid	Permeation Tube (output quantified by ion chromatography)	N/A	58	Neuman et al 1999
72.063	$C_3H_4O_2$	acrylic acid	Acrylic Acid	Liquid Standard supplied by Liquid Calibration Unit (LCU)	20	17	Mungall et al 2017
74.079	$C_3H_6O_2$	propionic acid	Propionic Acid	Liquid Standard supplied by Liquid	20	55	Mungall et al 2017

				Calibration Unit (LCU)			
79.011	HNO_4	pernitric acid	Pernitric Acid	Reaction of HO_2 with NO_2 (quantified by thermal decomposition Cavity Ringdown Spectroscopy of NO_2)	50	2	Veres et al 2015
84.074	$C_4H_4O_2$	$C_4H_4O_2$	2(5H)-Furanone	Liquid Standard supplied by Liquid Calibration Unit (LCU)	20	51	Mungall et al 2017
88.062	$C_3H_4O_3$	pyruvic acid	Pyruvic Acid	Liquid Standard supplied by Liquid Calibration Unit (LCU)	20	253	Mungall et al 2017
100.117	$C_5H_8O_2$	unsaturated C5 carboxylic acids	4-Pentenoic Acid	Liquid Standard supplied by Liquid Calibration Unit (LCU)	20	19	Mungall et al 2017
102.089	$C_4H_6O_3$	C4 oxo-carboxylic acids	2-Ketobutyric Acid	Liquid Standard supplied by Liquid Calibration Unit (LCU)	20	354	Mungall et al 2017
114.144	$C_6H_{10}O_2$	sum of cyclic saturated and n-unsaturated C5 carboxylic acids	Cyclopentan ecarboxylic Acid	Liquid Standard supplied by Liquid Calibration Unit (LCU)	20	28	Mungall et al 2017
116.116	$C_5H_8O_3$	C5 oxo-carboxylic acids	Levulinic Acid	Liquid Standard supplied by Liquid Calibration Unit (LCU)	20	11	Mungall et al 2017
126.155	$C_7H_{10}O_2$	unsaturated C6 cyclic carboxylic acid	3-Cyclohexene -1-carboxylic Acid	Liquid Standard supplied by Liquid Calibration Unit (LCU)	20	6	
132.159	$C_6H_{12}O_3$	C6 hydroxy-carboxylic acids	2-Hydroxyisoc aproic Acid	Liquid Standard supplied by Liquid Calibration Unit (LCU)	20	1.6	

382

383

384   Table S3. Standards used to calibrate the PTRMS. [a]C8 aromatics - expected contributions from ethyl
385   benzene, m- and p-xylenes and o-xylene. [b]Monoterpenes - expected contributions from camphene, α-
386   pinene, β-pinene, myrcene, and tricyclene.
387

Molecular weight	Molecular formula	Compound Name	Calibration standard
30.026	CH_2O	formaldehyde	formaldehyde
32.042	CH_4O	methanol	methanol
34.076	H_2S	hydrogen sulfide	hydrogen sulfide
41.053	C_2H_3N	acetonitrile	acetonitrile
44.053	C_2H_4O	acetaldehyde	acetaldehyde
56.064	C_3H_4O	acrolein	acrolein
58.08	C_3H_6O	acetone	acetone
62.13	C_2H_6S	dimethyl sulfide	dimethyl sulfide
68.119	C_5H_8	isoprene	isoprene
70.091	C_4H_6O	MVK, methacrolein, crotonaldehyde	crotonaldehyde
72.107	C_4H_8O	MEK, 2-methyl acetate, ethyl formate	methylethyl ketone
76.157	C_3H_8S	2-propanethiol, ethyl methyl sulfide	ethylmethyl sulfide
78.114	C_6H_6	benzene	benzene
84.136	C_4H_4S	thiophene	thiophene
90.184	$C_4H_{10}S$	diethyl sulfide, butanethiol	diethyl sulfide
92.141	C_7H_8	toluene	toluene
98.163	C_5H_6S	methyl thiophene	2-methylthiophene
106.168	C_8H_{10}	C8 aromatics[a]	o-xylene
112.19	C_6H_8S	dimethylthiophene	2,3-dimethylthiophene
136.238	$C_{10}H_{16}$	monoterpenes[b]	camphene

388

389   Table S4. Overlapping compounds measured between the PTRMS and AWAS.

Molecular Weight	Formula	Compound Name	Instrument	Decision for budget	Decision for EFs
42.081	C_3H_6	propene	AWAS and PTRMS	AWAS	AWAS
54.092	C_4H_6	butadiene/fragments	PTRMS	PTRMS	PTRMS and AWAS
		1,3-butadiene	AWAS		
56.108	C_4H_8	butenes	PTRMS	AWAS	AWAS
		cis-2-butene	AWAS		
		isobutene	AWAS		
		trans-2-butene	AWAS		
		1-butene	AWAS		
58.124	C_4H_{10}	butanes	PTRMS	AWAS	AWAS
		n-butane	AWAS		
68.119	C_5H_8	isoprene	PTRMS and AWAS	PTRMS	PTRMS and AWAS
70.135	C_5H_{10}	pentene/fragments	PTRMS	PTRMS	PTRMS and AWAS
		cis-2-pentene	AWAS		
		cyclopentane	AWAS		
		1-pentene	AWAS		
		2-methyl-1-butene	AWAS		
		2-methyl-2-butene	AWAS		
		3-methyl-1-butene	AWAS		
		t-2 pentene	AWAS		
82.146	C_6H_{10}	cyclohexene	PTRMS and AWAS	PTRMS	PTRMS
84.162	C_6H_{12}	hexene	PTRMS	PTRMS	PTRMS and AWAS
		cyclohexane	AWAS		
		cis-2-hexene	AWAS		
86.178	C_6H_{14}	hexanes	PTRMS	AWAS	AWAS
		n-hexane	AWAS		
		2,3-dimethyl butane	AWAS		
		2,3-dimethylpentane	AWAS		

390

391

392   Table S5. Overlapping compounds measured between the PTRMS and CIMS.

Molecular weight	Formula	CIMS compound name	PTRMS compound name	Decision
43.025	HNCO	Isocyanic acid	Isocyanic acid	CIMS and PTRMS for reporting EF and ER; CIMS for carbon budget
46.025	CH_2O_2	Formic acid	Formic acid	CIMS
57.052	C_2H_3NO	Hydroxy acetonitrile	Methyl isocyanate	CIMS and PTRMS
60.052	$C_2H_4O_2$	Acetic acid	Acetic acid	CIMS and PTRMS for reporting EF and ER; CIMS for carbon budget
72.063	$C_3H_4O_2$	Acrylic acid	Methyl glyoxal/acrylic acid	CIMS
74.079	$C_3H_6O_2$	Propionic acid	Hydroxy acetone/ethyl formate	CIMS and PTRMS
84.074	$C_4H_4O_2$	Unidentified	Furanone	CIMS and PTRMS
85.062	$C_3H_3NO_2$	Cyanoacetic acid	Methyl cyanoformate	CIMS and PTRMS
86.09	$C_4H_6O_2$	Methacrylic acid	Butanedione/isomers	CIMS and PTRMS
88.106	$C_4H_8O_2$	C4 saturated carboxylic acids	Methyl propanoate	CIMS and PTRMS
100.117	$C_5H_8O_2$	Unsaturated C5 carboxylic acids	Methyl methacrylate/isomers	CIMS and PTRMS
102.089	$C_4H_6O_3$	C4 oxo-carboxylic acids	Acetic anhydride	CIMS and PTRMS
102.133	$C_5H_{10}O_2$	C5 saturated carboxylic acids	Valeric acid	CIMS and PTRMS
114.144	$C_6H_{10}O_2$	Sum of cyclic saturated and n-saturated C5 carboxylic acids	Caprolactone/c6 esters/c6diketone isomers	CIMS and PTRMS
116.16	$C_6H_{12}O_2$	C6 carboxylic acids	Butyl acetate/c6 esters	CIMS and PTRMS
118.132	$C_7H_{10}O_2$	Unsaturated C6 cyclic carboxylic acids	Cyclohexene carboxylic acid	CIMS and PTRMS
128.171	$C_7H_{12}O_2$	C6 unsaturated carboxylic acids	Cyclohexanoic acid	CIMS and PTRMS
130.187	$C_7H_{14}O_2$	C7 saturated carboxylic acids	Amyl acetate	CIMS and PTRMS

393

394

Table S6. Compounds with no significant observed emissions

Molecular Weight	Formula	Compound Name	Instrument
34.08	H_2S	hydrogen sulfide	PTRMS
70.05	$C_2H_3O_2$	Propiolic acid	PTRMS
72.17	C_5H_{12}	2,2-dimethylpropane	AWAS
82.06	$C_4H_2O_2$	cyclobutenedione	PTRMS
85.06	$C_3H_3NO_2$	cyanoacetic acid	CIMS
86.2	C_6H_{14}	2,2-dimethylbutane	AWAS
91.07	$C_2H_5NO_3$	C2 nitro alcohol	CIMS
100.07	$C_4H_4O_3$	dihydro furandione	PTRMS
102.195	$C_5H_{10}S$	cyclopentanethiol	PTRMS
104.105	$C_4H_8O_3$	C4 hydroxy-carboxylic acids	CIMS
112.24	C_8H_{16}	cis-1,2-dimethylcyclohexane	AWAS
112.56	C_6H_5Cl	chlorobenzene	PTRMS
118.13	$C_5H_{10}O_3$	C5 hydroxy-carboxylic acids	CIMS
128.29	C_9H_{20}	2,5-dimethylheptane	AWAS
134.24	$C_{10}H_{14}$	1-methyl-2-n-propylbenzene	AWAS
140.25	$C_8H_{12}S$	butylthiophene	PTRMS
142.32	$C_{10}H_{22}$	2,2-dimethyloctane	AWAS
147.00	$C_6H_4Cl_2$	dichlorobenzene	PTRMS
154.12	$C_7H_6O_4$	dihydroxybenzoic acid	PTRMS
n/a	Cl^-	p-chloride	AMS

409   Table S7. Emission ratios (relative to CO, as µg m^{-3} of I/SVOC per µg m^{-3} CO) for complex mixtures of
410   gas-phase CH, CHO$_1$, and CHS$_1$ compounds grouped by carbon number for all targeted molecular
411   formulas, derived from the integrated cartridge samples, using the sample taken across the lowest
412   transects of Screen 1. The ERs are reported as a range with the lower limit reflecting the subtraction of a
413   slightly contaminated background, and the upper limit having no background subtracted.

Carbon Number	CH (µg m^{-3})/ CO (µg m^{-3})	CHO$_1$ (µg m^{-3})/ CO (µg m^{-3})	CHS$_1$ (µg m^{-3})/ CO (µg m^{-3})
10	1.1E-02 - 1.1E-02	3.2E-03 - 3.2E-03	7.2E-06 - 7.9E-06
11	0.0E+00 - 0.0E+00	6.6E-04 - 6.6E-04	1.6E-05 - 1.6E-05
12	5.4E-05 - 5.4E-05	4.6E-04 - 7.4E-04	0.0E+00 - 2.4E-06
13	3.3E-06 - 2.4E-04	4.4E-05 - 5.4E-04	9.2E-06 - 1.4E-05
14	5.3E-05 - 1.6E-04	3.7E-04 - 1.1E-03	4.4E-06 - 5.8E-06
15	6.0E-05- 3.7E-04	3.3E-04 - 1.0E-03	2.2E-05 - 2.4E-05
16	3.4E-04 - 1.1E-03	3.6E-04 – 7.0E-04	5.4E-05 - 6.8E-05
17	7.6E-04 - 1.2E-03	1.2E-03 - 1.9E-03	3.3E-04 - 3.4E-04
18	1.0E-03 - 1.7E-03	2.1E-04 - 1.3E-03	1.2E-04 - 1.2E-04
19	1.6E-03 - 1.9E-03	5.7E-04 -1.2E-03	3.9E-04 - 4.3E-04
20	1.9E-03 - 2.8E-03	3.1E-04 - 9.1E-04	1.1E-04 - 1.4E-04
21	2.5E-03 - 2.5E-03	2.6E-04 - 5.2E-04	2.3E-04 - 2.9E-04
22	3.8E-03 - 4.0E-03	1.7E-04 - 3.3E-04	1.9E-05 - 8.9E-05
23	2.1E-03 - 2.2E-03	6.7E-05 - 1.5E-04	2.9E-05 - 2.9E-05
24	7.6E-04 - 1.0E-03	3.3E-05 - 1.2E-04	4.4E-05 - 6.0E-05
25	4.0E-04 - 4.3E-04	9.0E-06 - 5.5E-05	1.3E-05 - 6.1E-05

414

415

416

417

418

419

420

421

422

423

424

425

426   Table S8. Compounds shown in Fig. 9 where the identifications/naming are not exact matches with the
427   current study. 1 Individually identified compounds were summed for comparison to the present study; 2
428   Each compound was compared with the value from the present study.

Molecular Weight	Compound	Instrument	Compound Name	Andreae Names	Koss Names	Permar Names	Urbanski Names
54.092	C_4H_6	PTRMS	butadiene/fragments	butadiene	1,3-butadiene + 1,2-butadiene	1,3-butadiene, 1,2-butadiene	n/a
54.092	C_4H_6	AWAS	1,3-butadiene	butadiene	1,3-butadiene + 1,2-butadiene	1,3-butadiene, 1,2-butadiene	n/a
57.052	C_2H_3NO	CIMS	hydroxy acetonitrile	n/a	methyl isocyanate + hydroxyacetonitrile	methyl isocyanate, hydroxyacetonitrile	n/a
58.124	C_4H_{10}	AWAS	isobutane	n/a	n/a	n-Butane	n/a
60.052	$C_2H_4O_2$	CIMS	acetic acid	Acetic acid	acetic acid + glycolaldehyde	acetic acid, glycolaldehyde (=hydroxylacetaldehyde)	n/a
60.096	C_3H_8O	PTRMS	propanol	n/a	n/a	Isopropanol	n/a
66.103	C_5H_6	PTRMS	cyclopentandiene	n/a	n/a	1,3-cyclopentadiene	1,3-CyclopentadienePIT
70.091	C_4H_6O	PTRMS	MVK, methacrolein, crotonaldehyde	Methacrolein	MVK + methacrolein + crotonaldehyde	Methyl vinyl ketone, Methacrolein, 2-Butenal (=crotonaldehyde)	[1]Crotonaldehyde + Methacrolein + Methyl Vinyl Ketone MVK
70.135	C_5H_{10}	PTRMS	pentene/methyl butene/fragments	1-Pentene + 2-pentene	pentene+methyl butene	pentenes, methylbutenes	n/a
70.135	C_5H_{10}	AWAS	c-2-pentene	2 pentene cis&tran	pentene+methyl butene	pentenes, methylbutenes	n/a
70.135	C_5H_{10}	AWAS	cyclopentane			cyclopentane	n/a
70.135	C_5H_{10}	AWAS	1-pentene	1-Pentene	pentene+methyl butene	pentenes, methylbutenes	n/a
70.135	C_5H_{10}	AWAS	methyl-1-butene	1-Pentene	pentene+methyl butene	pentenes, methylbutenes	n/a
70.135	C_5H_{10}	AWAS	methyl-2-butene	1-Pentene	pentene+methyl butene	pentenes, methylbutenes	n/a
72.063	$C_3H_4O_2$	CIMS	acrylic acid	n/a	n/a	pyruvaldehyde (=methyl glyoxal), acrylic acid	n/a
72.107	C_4H_8O	PTRMS	methy ethyl ketone + butanal + 2-methylpropanal	2-butanone (methyl ethyl ketone)	methyl ethyl ketone + butanal + 2-methylpropanal	methyl ethyl ketone, 2-methylpropanal, butanal	[1]Methyl Ethyl Ketone MEK + n-Butanal + 2-

							Methylpropanal
72.151	C_5H_{12}	AWAS	methylbutane	n/a	n/a	n-pentane	n/a
74.079	$C_3H_6O_2$	PTRMS	hydroxy acetone/ethyl formate	n/a	methyl acetate + ethyl formate + hydroxyacetone	Hydroxyacetone, Methyl acetate, Ethyl formate	Ethyl Formate
81.118	C_5H_7N	PTRMS	pentene nitriles/methyl pyrrole	n/a	n/a	n/a	1-Methylpyrrole
82.102	C_5H_6O	PTRMS	methyl furan	n/a	2-methylfuran + 3-methylfuran + general HCO	2-Methylfuran, 3-Methylfuran	[2]2-Methylfuran, 3-Methylfuran
84.118	C_5H_8O	PTRMS	cyclopentanone/ isomers	n/a	3-methyl-3-butene-2-one + cyclopentanone + HCO1 isomers	3-Methyl-3-buten-2-one, Cyclopentanone	Cyclopentanone
84.162	C_6H_{12}	PTRMS	hexene/fragments	1-hexene	n/a	n/a	[2]1-Hexene, cis-2-Hexene
86.09	$C_4H_6O_2$	PTRMS	butanedione/ isomers	2,3-butanedione	2,3-butanedione + methyl acrylate + other HCO2	2,3-butanedione, methyl acrylate	2,3-Butadione
86.134	$C_5H_{10}O$	PTRMS	pentanone	n/a	n/a	n/a	[2]2-Pentanone, 3-Pentanone
86.178	C_6H_{14}	AWAS	2+3-methylpentane	n/a	n/a	3-methylpentane	3-Methylpentane
96.085	$C_5H_4O_2$	PTRMS	furfural	furfural (2-furaldehyde)	2-furfural + 3-furfural + other HCO2	2-furfural (=furaldehyde), 3-furfural	2-Furaldehyde
98.189	C_7H_{14}	PTRMS	heptene	n/a	n/a	n/a	1-Heptene
100.117	$C_5H_8O_2$	PTRMS	methyl methacrylate / isomers	n/a	Methyl methacrylate + other HCO2	Methyl methacrylate	Methyl Methacrylate
100.161	$C_6H_{12}O$	PTRMS	hexanal/hexanones	n/a	hexanal + hexanones	Hexanones, Hexanal	[1]n-Hexanal + Hexanones
103.124	C_7H_5N	PTRMS	benzonitrile	n/a	Benzonitrile	Benzonitrile	Benzenenitrile
106.168	C_8H_{10}	PTRMS	C8 aromatics	n/a	Ethyl benzene + m-xylene + p-	C8 Aromatics	[1]Ethylbenzene + m,p-Xylenes + o-Xylene

					xylene + o-xylene		
112.216	C_8H_{16}	PTRMS	octene	n/a	n/a	n/a	1-Octene
118.135	C_8H_6O	PTRMS	benzofuran	n/a	Benzofuran	Benzofuran	BenzofuranPIT
118.179	C_9H_{10}	PTRMS	methylstyrenes/ propenyl benzenes	n/a	Indane + methyl styrenes + propenyl benzenes	Methylstyrenes, Indane, Propenylbenzenes	[1]1-Propenylbenzene, 2-Methylstyrene, 2-Propenylbenzene, 3-Methylstyrene, 4-Methylstyrene, alpha-Methylstyrene
120.195	C_9H	PTRMS	C9 aromatics	1,2,3-trimethylbenzen, 1,2,4-trimethylbenzen, 1,3,5-trimethylbenzene (Simpson et al., 2011)	C9 aromatics	C9 aromatics	[1]1,2,3-Trimethylbenzene, 1,2,4-Trimethylbenzene, 1,3,5-Trimethylbenzene, 1-Ethyl-2-Methylbenzene, 1-Ethyl-3-,4-Methylbenzene, Isopropylbenzene, n-Propylbenzene
132.162	C_9H_8O	PTRMS	methyl benzo furans	n/a	Methyl benzofuran	Methylbenzofurans	[1]Methylbenzofuran isomer 1, Methylbenzofuran isomer 2, Methylbenzofuran isomer 3
132.206	$C_{10}H_{12}$	PTRMS	ethyl styrene/ methyl propenyl benzene	n/a	Methyl propenyl benzene + ethyl styrene	Ethyl styrenes, Methylpropenylbenzenes, Butenylbenzenes	[1]1-Methyl-1-Propenylbenzene, Ethylstyrene
134.222	$C_{10}H_{14}$	PTRMS	C10 Aromatics	n/a	C10 Aromatics	C10 Aromatics	[1]1,4-Diethylbenzene,

							1-Butenylbenzene, Ethyl Xylene isomer 1, Ethyl Xylene isomer 2, Isobutylbenzene, Methyl-n-Propylbenzene isomer 1, Methyl-n-Propylbenzene isomer 2, n-Butylbenzene, p-Cymene
136.238	$C_{10}H_{16}$	PTRMS	monoterpenes	sum of alpha + beta-pinene (Simpson et al., 2011)	monoterpenes	monoterpenes	n/a
148.249	$C_{11}H_{16}$	PTRMS	C11 aromatics/ pentamethyl benzene	n/a	n/a	n/a	C11 Aromatics

429

430

431   Table S9. Emission speciation profile for SAPRC11 chemical mechanism derived from normalized EFs
432   from the present study and compared with wildfire smoldering emission speciation profile from the EPA
433   SPECIATEv4.5 #95428 dataset. Note that SESQ (sesquiterpene), WSOC (water soluble organic carbon)
434   and IVOC are non-standard SAPRC11 mechanism species. Please refer to Carter and Heo (2013) for
435   mechanism species definition.

SAPRC11 Lumped Species Name	Molecular Weight (g/mol)	Normalized Mass Fraction (Hayden et al.)	Normalized Mass Fraction (SPECIATEv4.5 #95428)
CCOOH	60.05	0.038	0.031
ACET	58.08	0.024	0.0072
ACYL	26.04	0.0080	0.00059
ALK1	30.07	0.039	0.011
ALK2	36.73	0.013	0.0043
ALK3	58.61	0.0063	0.0077
ALK4	77.6	0.0055	0.030
ALK5	118.89	0.0053	0.28
ARO1	95.16	0.031	0.034
ARO2	118.72	0.042	0.067
BACL	86.09	0.021	0.0050
BALD	106.13	0.0020	0.0034
BENZ	78.11	0.013	0.0035
CATL	110.1	0.0032	0.014
CCHO	44.05	0.032	0.023
CH4	16.043	0.24	0.044
CRES	108.14	0.0026	0.0027
ETHE	28.05	0.044	0.0065
HCOOH	46.03	0.0050	0.0038
GLY			0.000046
HCHO	30.03	0.030	0.0084
IPRD	100.12	0.00020	0.0037
ISOP	68.12	0.021	0.00041
MACR	70.09	0.010	0.0044
MEK	72.11	0.0066	0.0028
MEOH	32.04	0.057	0.016
MGLY			0.000037
MVK	70.09	0.0057	0.019
NROG	1	0.11	0.13
NVOL	1	1.18E-05	
OLE1	72.34	0.079	0.049
OLE2	75.78	0.019	0.025
PACD	74.08	0.055	0.00047
PHEN	94.11	0.0055	0.0054
PROD2	116.16	0.0044	0.027

RCHO	58.08	0.038	0.0035
TERP	136.24	0.024	0.032
XYNL	122.16	0.0080	
SESQ	204.35	0.039	
WSOC	227	0.013	
IVOC	227.3	0.0063	

436

437
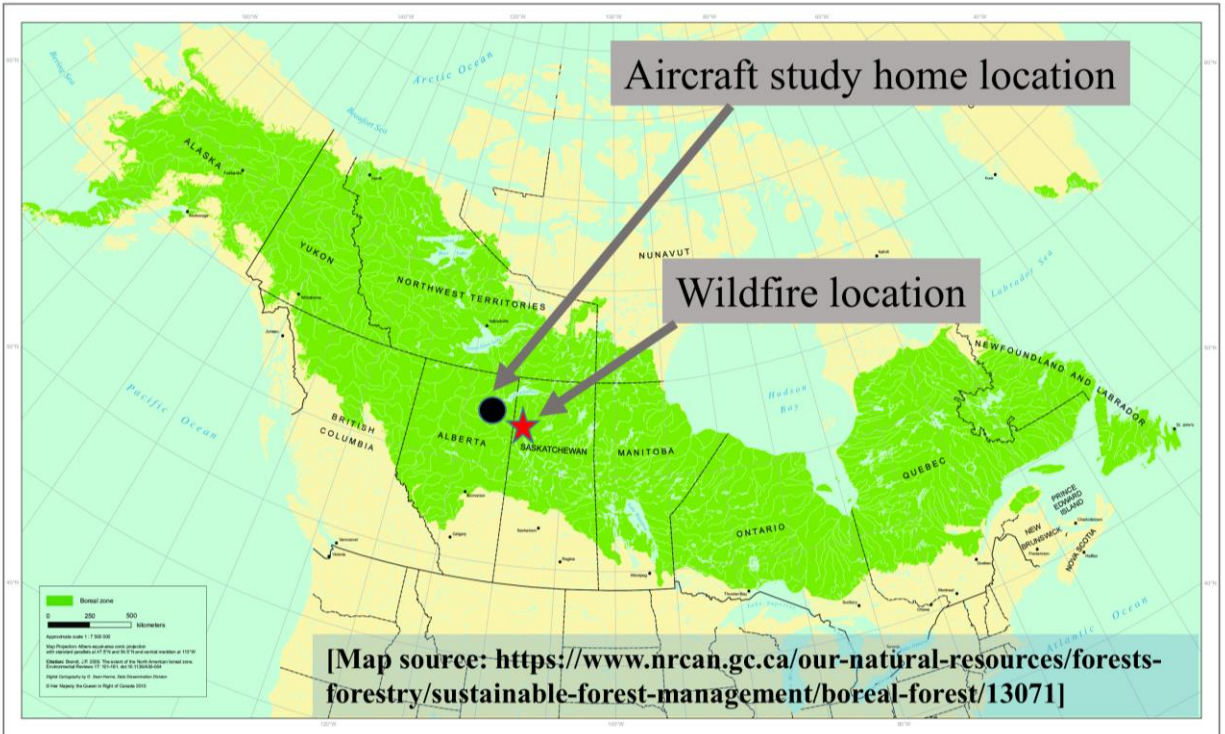
438

439   Figure S1. Map showing the home location of the airborne study at Fort McMurray, Alberta and the
440   location of the wildfire in Saskatchewan. The green shaded region shows the extent of the boreal forest
441   coverage across Canada and Alaska.

442

443
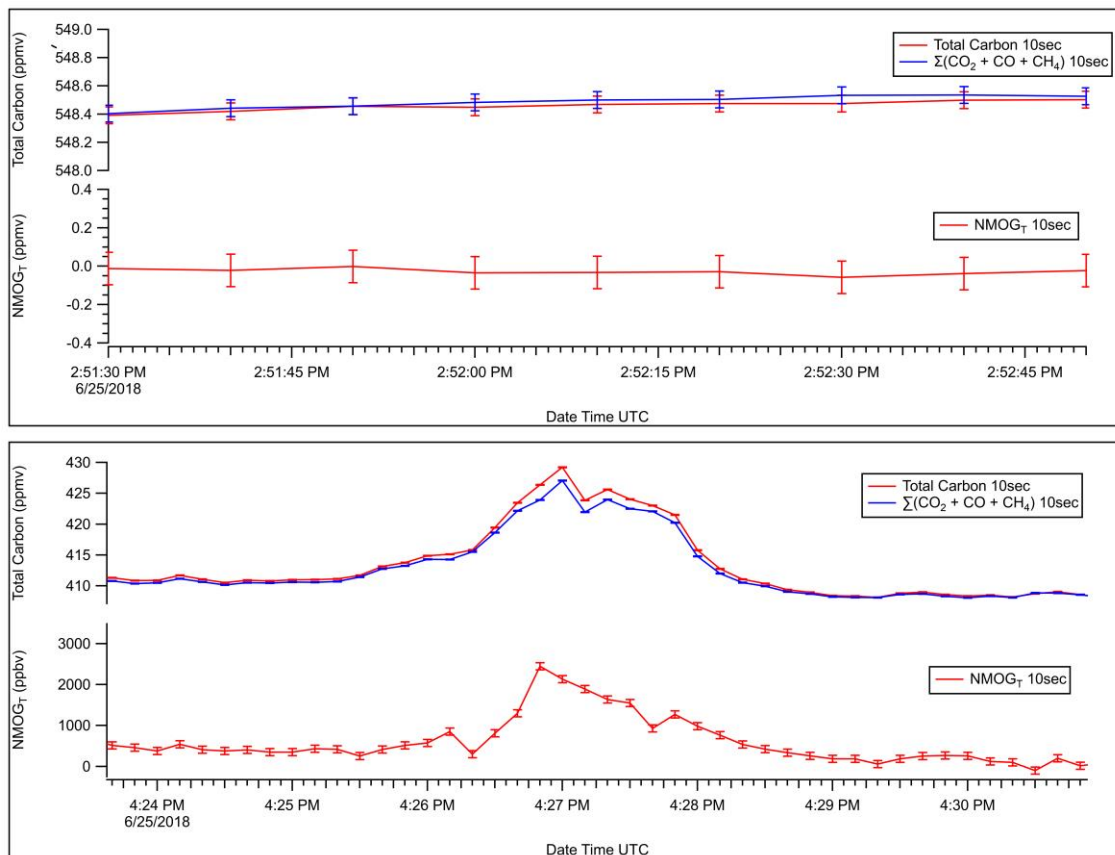
Figure S2. Total carbon (TC), $\Sigma(CO_2+CO+CH_4)$ (ppmv C), and $NMOG_T$ (ppmv C or ppbv C) averaged to 10 sec for a) a portion of the in-flight calibration time period, and b) a selected plume along Screen 1. $NMOG_T$, the difference between the TC and $\Sigma(CO_2+CO+CH_4)$, has an uncertainty of ±85 ppbv C.

444
445
446

447

448

449

450

451

452

453

454

455

456

457

458
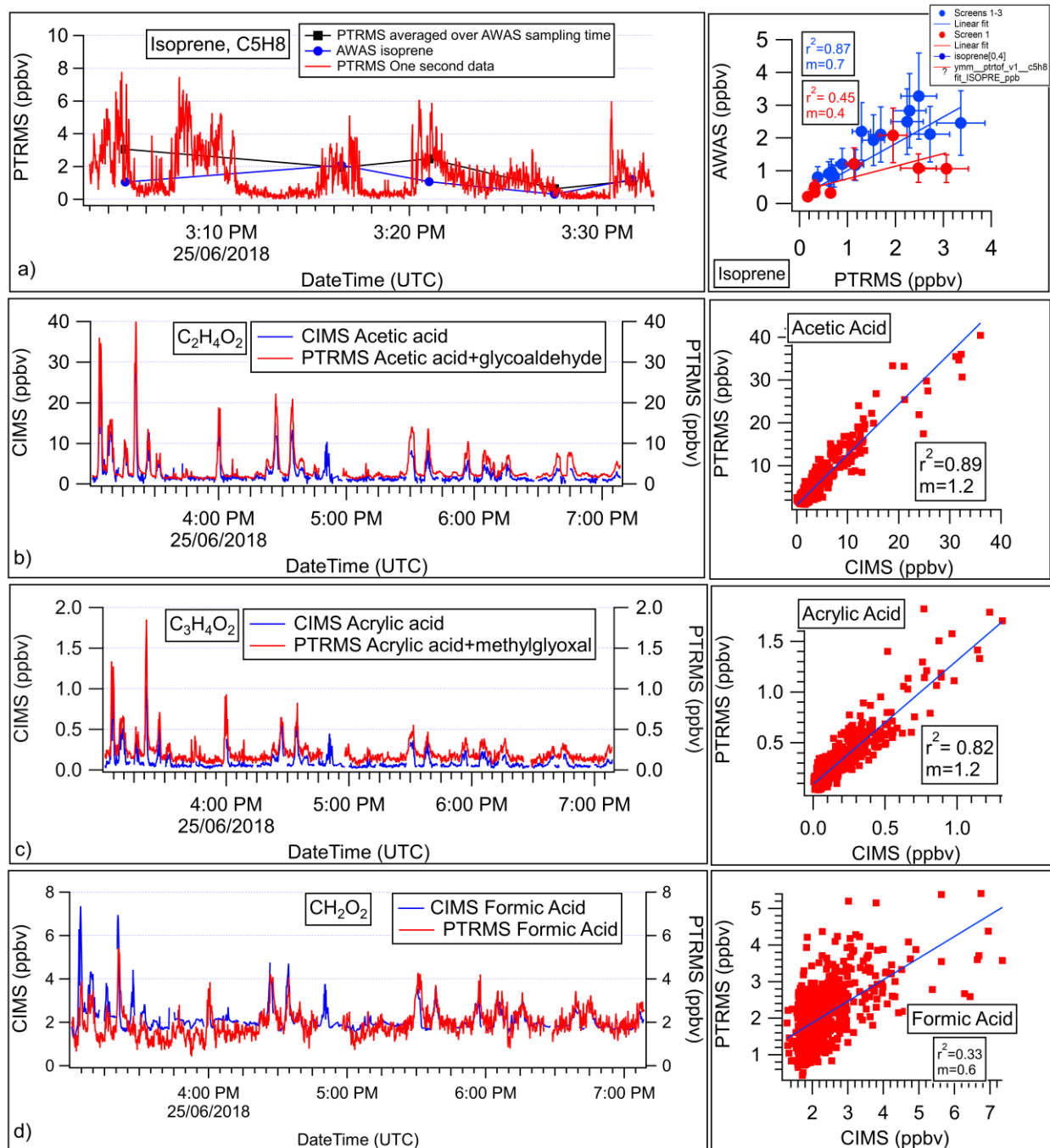
Figure S3. Intercomparisons of overlapping compounds between the PTRMS and AWAS, and between the PTRMS and CIMS for a) isoprene, b) acetic acid, c) acrylic acid, and d) formic acid.

466
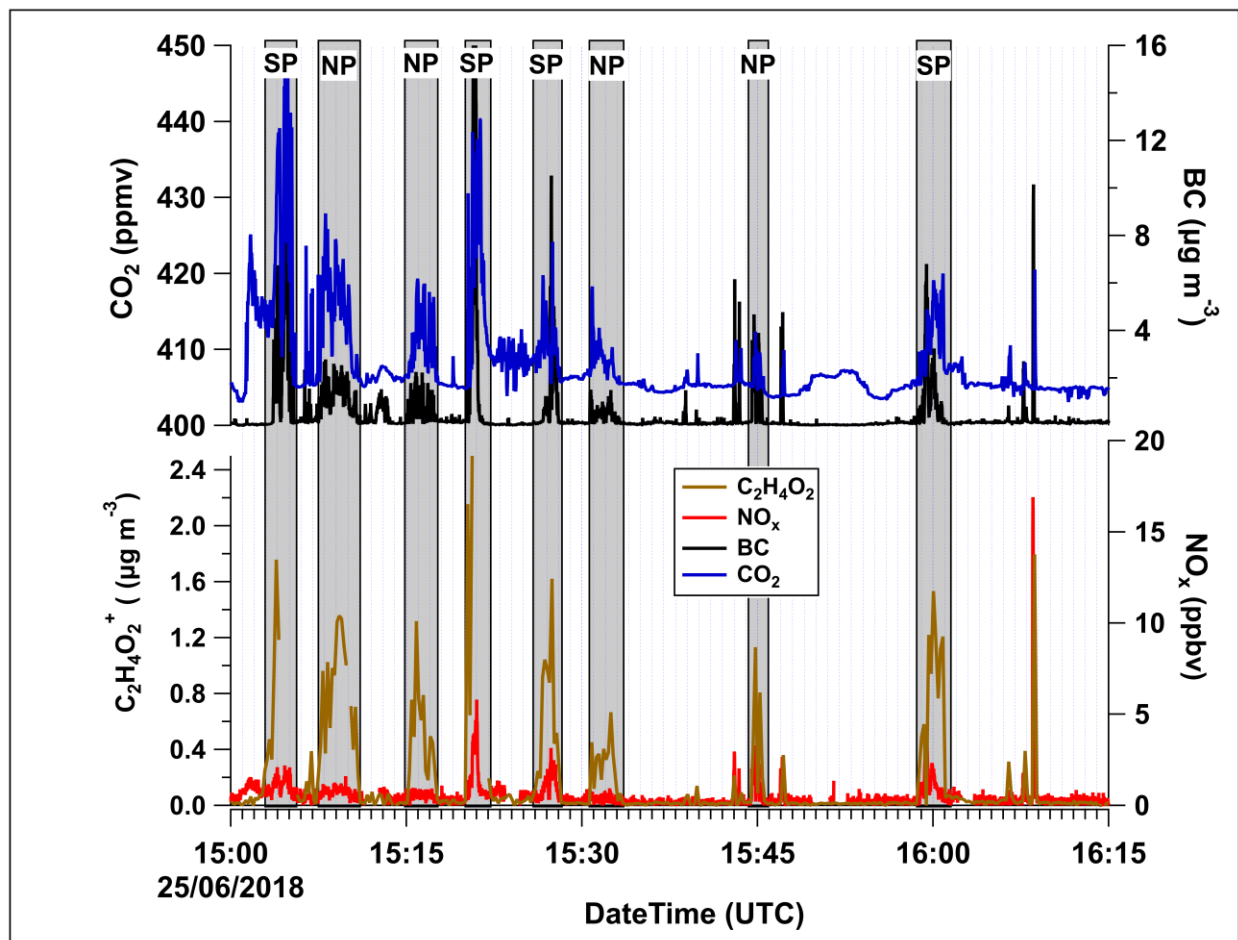
Figure S4. Time series of CO_2, BC and NO_x mixing ratios, and $C_2H_4O_2^+$ (levoglucosan fragment derived
from the AMS) concentrations for Screen 1. The in-plume portions are indicated by the vertical grey
bars. The aircraft flew back and forth across the plumes at increasing altitudes to complete five transects;
a transect represents one pass across the SP and NP at the same altitude.

467
468
469
470

471

472

473

474

475

476

477

478

479

480
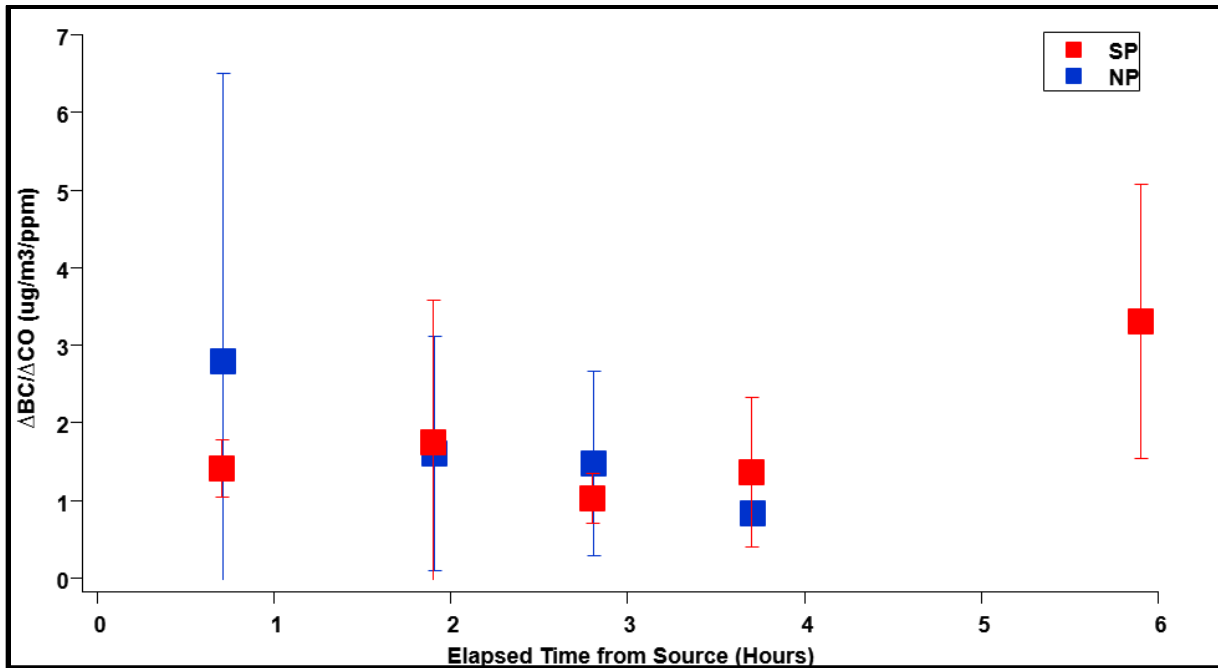
481

482 Figure S5. Using ΔBC/ΔCO (Selimovic et al., 2019) as an indicator of plume mixing downwind of the
483 Lac LaLoche fire. The squares show the average and the vertical lines the standard deviation for the
484 transects within the mixed layer for each screen.

485

S1 NP

- OA
- BC
- NH4
- SO4
- NO3

92.6%

2.9%
1.5%
1.2%
1.8%

S1 SP

- OA
- BC
- NH4
- SO4
- NO3

90.4%

3.6%
1.9%
1.4%
2.7%
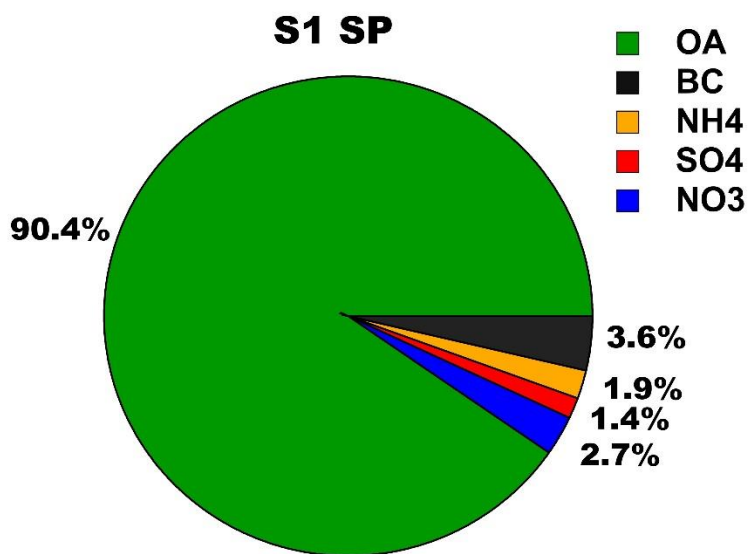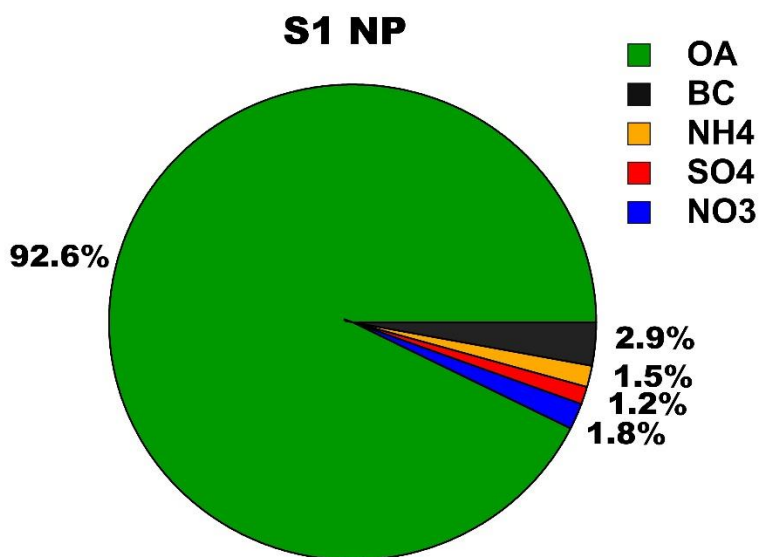
486

487   Figure S6. Percent contribution from individually measured particle-phase species for the NP and SP

488   including p-organics (OA), black carbon (BC), ammonium (NH_4), sulphate (SO_4) and nitrate (NO_3), based

489   on mass concentrations.

490

491

492
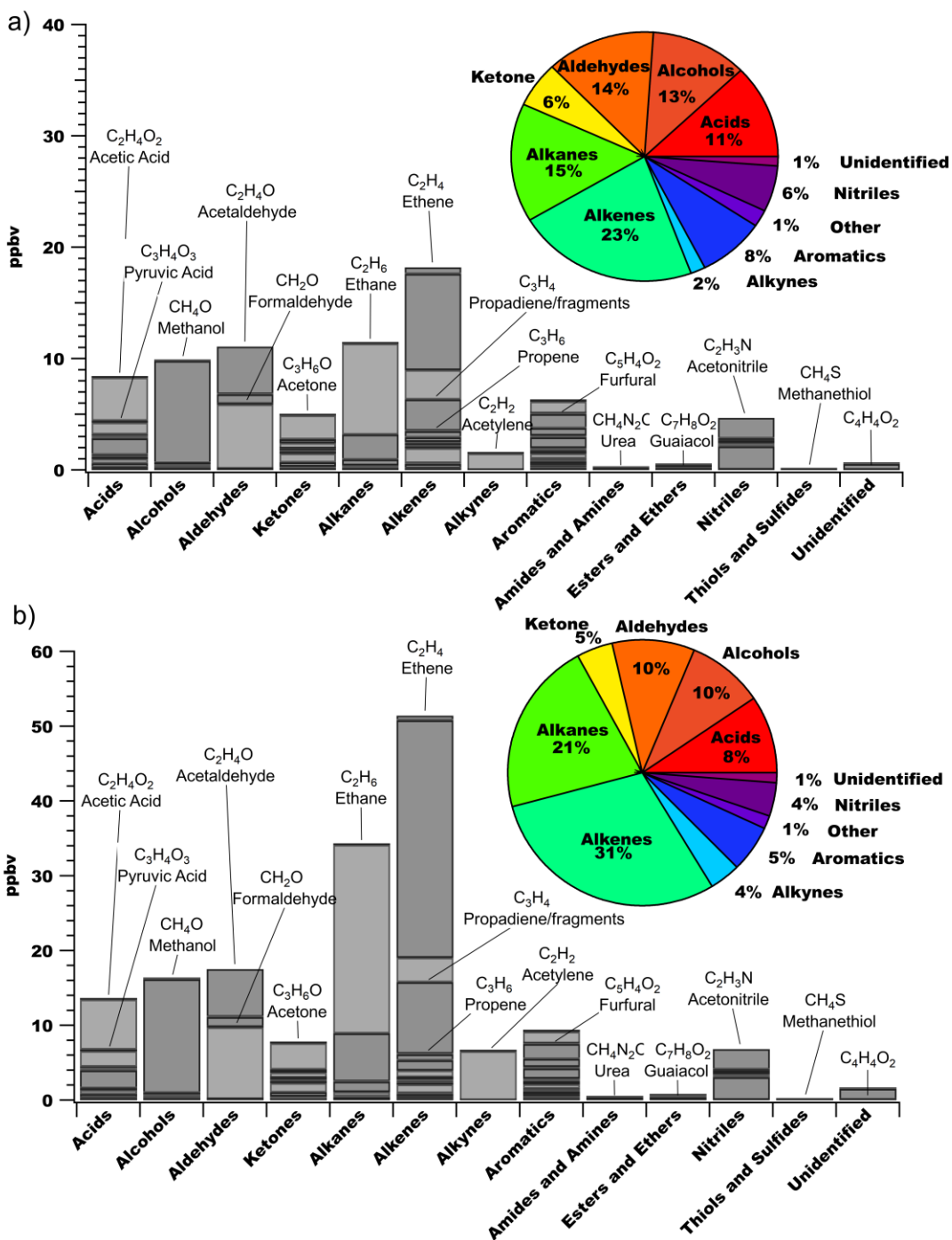
Figure S7. Background-subtracted mixing ratios of individually measured NMOGs from the PTRMS, CIMS and AWAS are shown for thirteen chemical classes for the a) NP and b) SP. In some cases, compounds are double- (or triple-) counted if they can be identified in more than one category. For example, phenol is an alcohol + an aromatic; guaiacol is an alcohol + an ether + an aromatic. In the pie chart, the *Other* category includes amides, amines, ethers, thiols and sulfides. The *Unidentified* category contains molecular formulas detected but the compound(s) could not be identified.
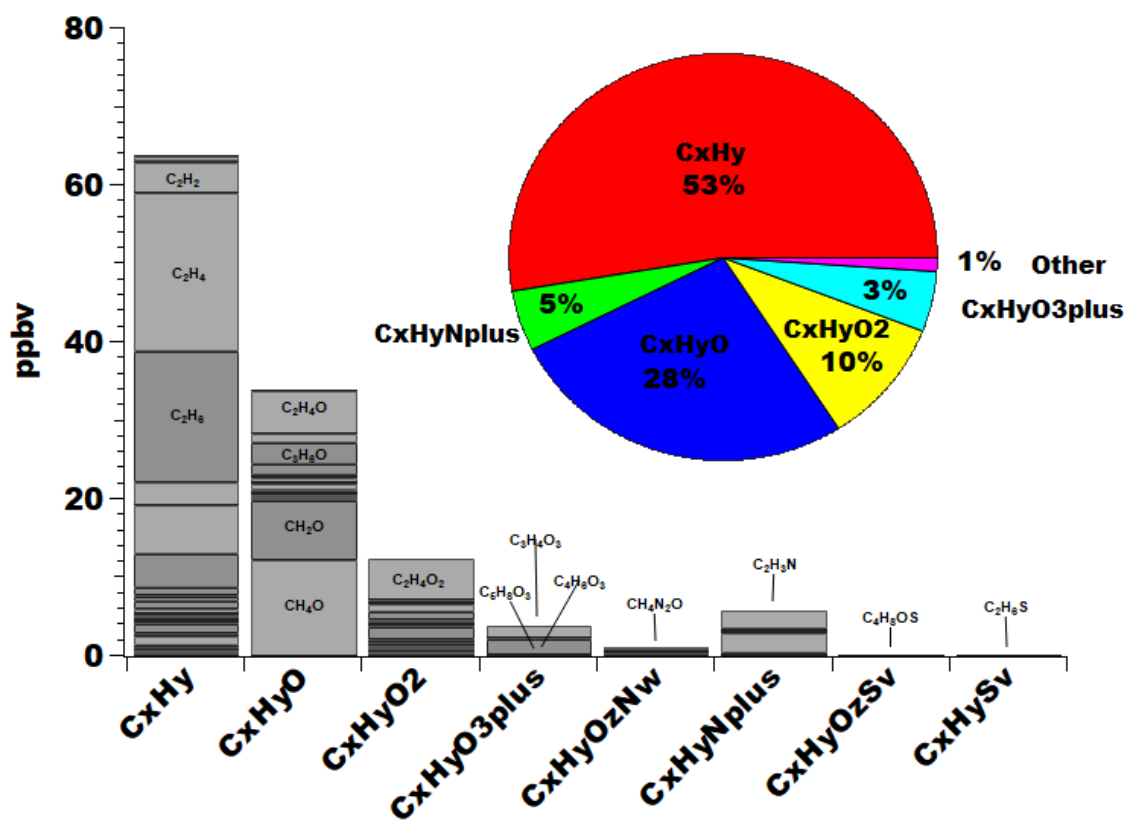
Figure S8. Background-subtracted average mixing ratios of individually measured NMOGs from the PTRMS, CIMS and AWAS are shown for molecular formulae classes. The *Unidentified* category contains molecular formulas detected but the compound(s) could not be identified.

504
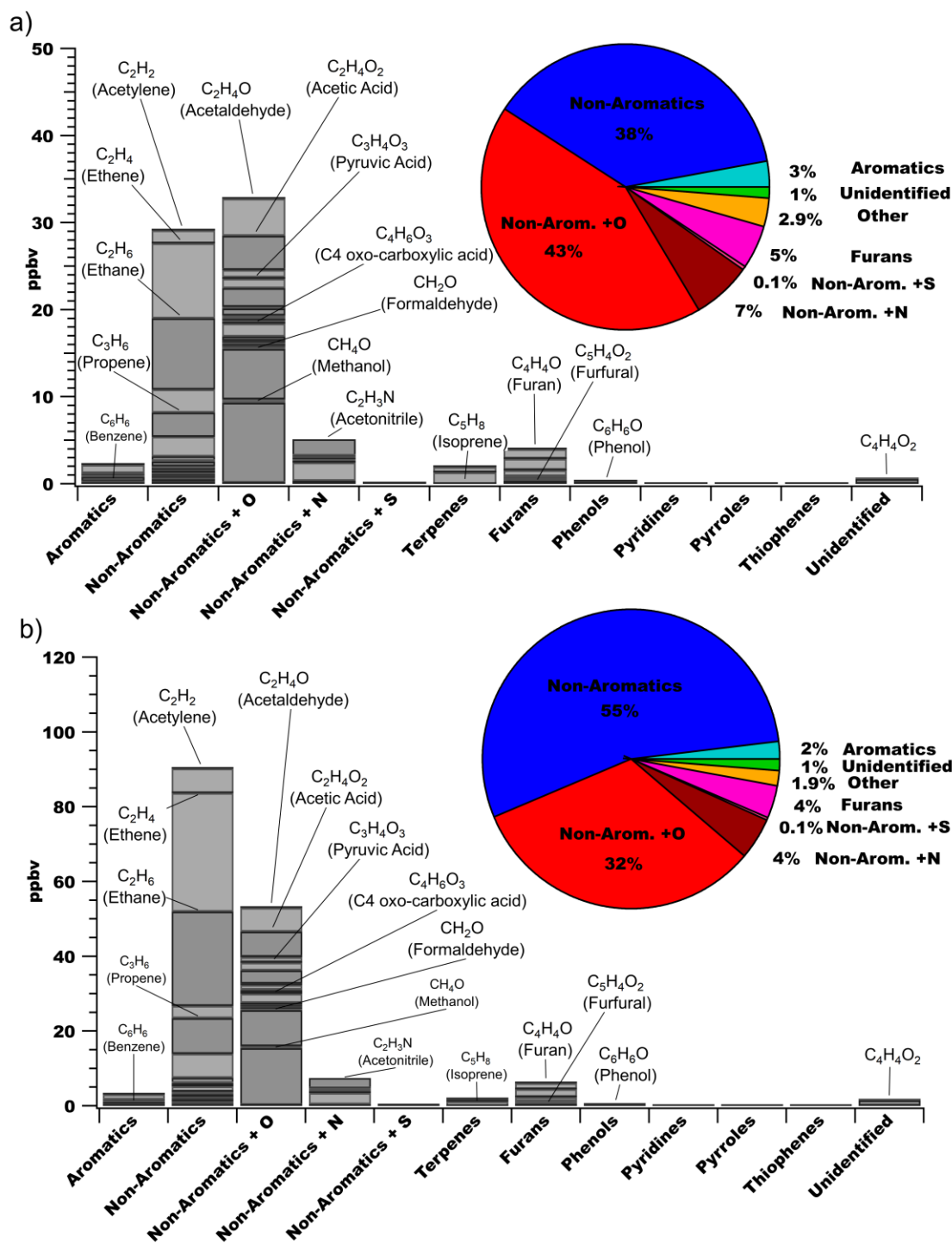
Figure S9. Average mixing ratios of individually measured NMOGs from the PTRMS, CIMS and
AWAS by structural group for the a) NP and b) SP. The *Other* category is the sum of terpenes, phenols,
pyridines, pyrroles and thiophenes.

508

509

South Plume

NMOG EF = 25.5 ± 3.6 g C kg^{-1}
VOCs (PTR+CIMS+AWAS) = 13.1 ± 1.0 g C kg^{-1}
IVOC/SVOCs (Cartridge) = 2.1 to 3.0 g C kg^{-1}
Unidentified = 9.4 ± 3.7 to 10.3 ± 3.7 g C kg^{-1}

Low IVOC/SVOCs Range

High IVOC/SVOCs Range

91.6% 6.3% 0.5% 1.5%

51 ± 4% 8% 41 ± 14.5%

51 ± 4% 12% 37 ± 14.5%

- CO_2 - NMOG
- CO   - VOCs (PTR+CIMS+AWAS)   - IVOC/SVOCs (Cartridge)
- CH_4 - Unidentified

89.6% 7.7% 0.5% 2.2%

38 ± 2% 6% 56 ± 16%

38 ± 2% 8% 54 ± 16%

Low IVOC/SVOCs Range

High IVOC/SVOCs Range

North Plume

NMOG EF = 36.8 ± 5.6 g C kg^{-1}
VOCs (PTR+CIMS+AWAS) = 13.9 ± 0.8 g C kg^{-1}
IVOC/SVOCs (Cartridge) = 2.1 to 3.0 g C kg^{-1}
Unidentified = 19.9 ± 5.7 to 20.8 ± 5.7 g C kg^{-1}

510

511   Figure S10. Percent contributions of carbon-containing compounds to the TC based on EFs (in terms of
512   carbon fraction) for the SP and NP. The two pie charts on the right, representing the low and high
513   I/SVOC EF estimates, show the percent breakdown of the measured NMOGs and the remaining
514   unidentified portion. The EF values (g C kg^{-1}) are identified in the boxes. Note, the I/SVOC
515   measurements represent the integrated average encompassing both plumes.
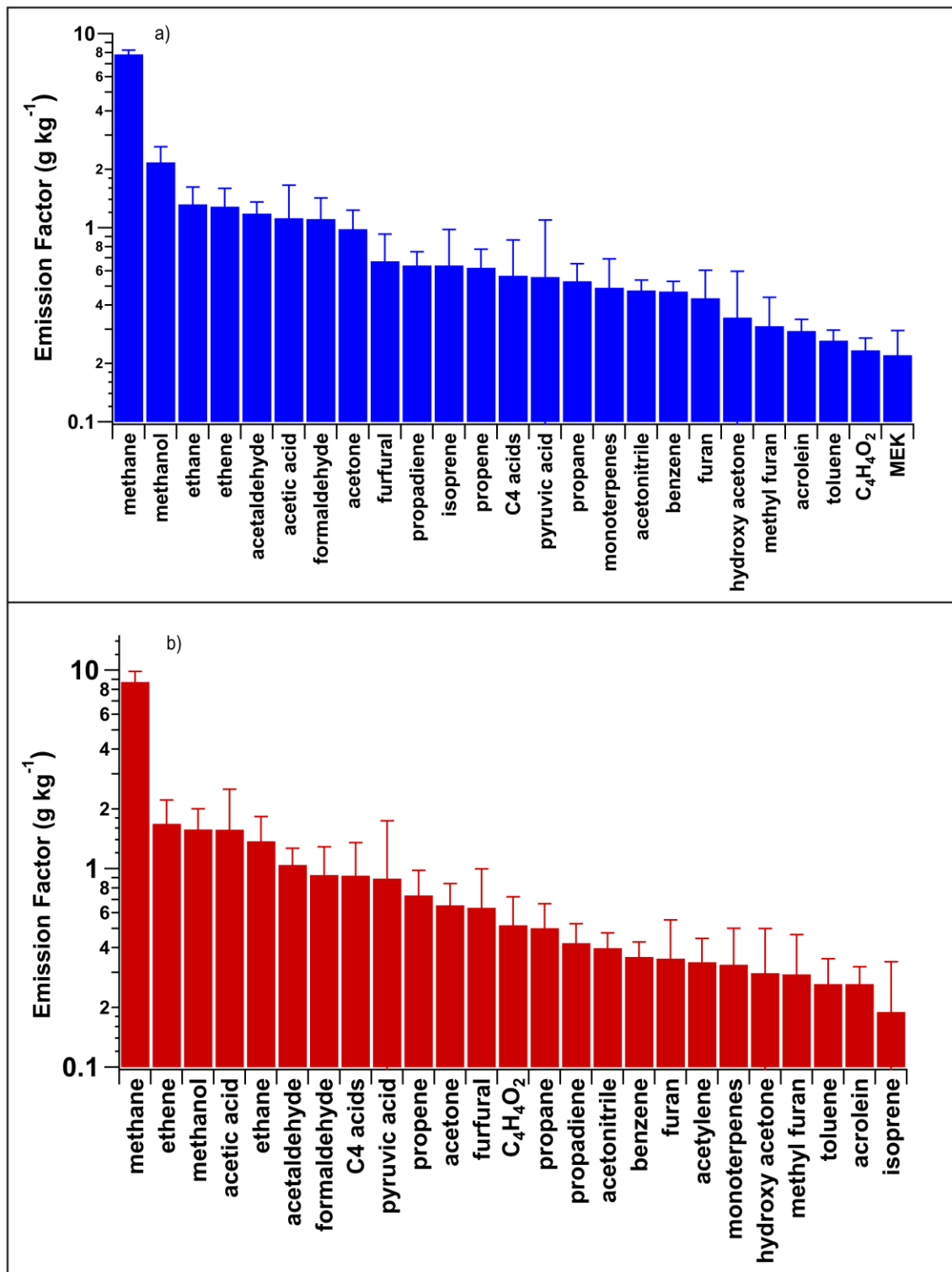
516

517
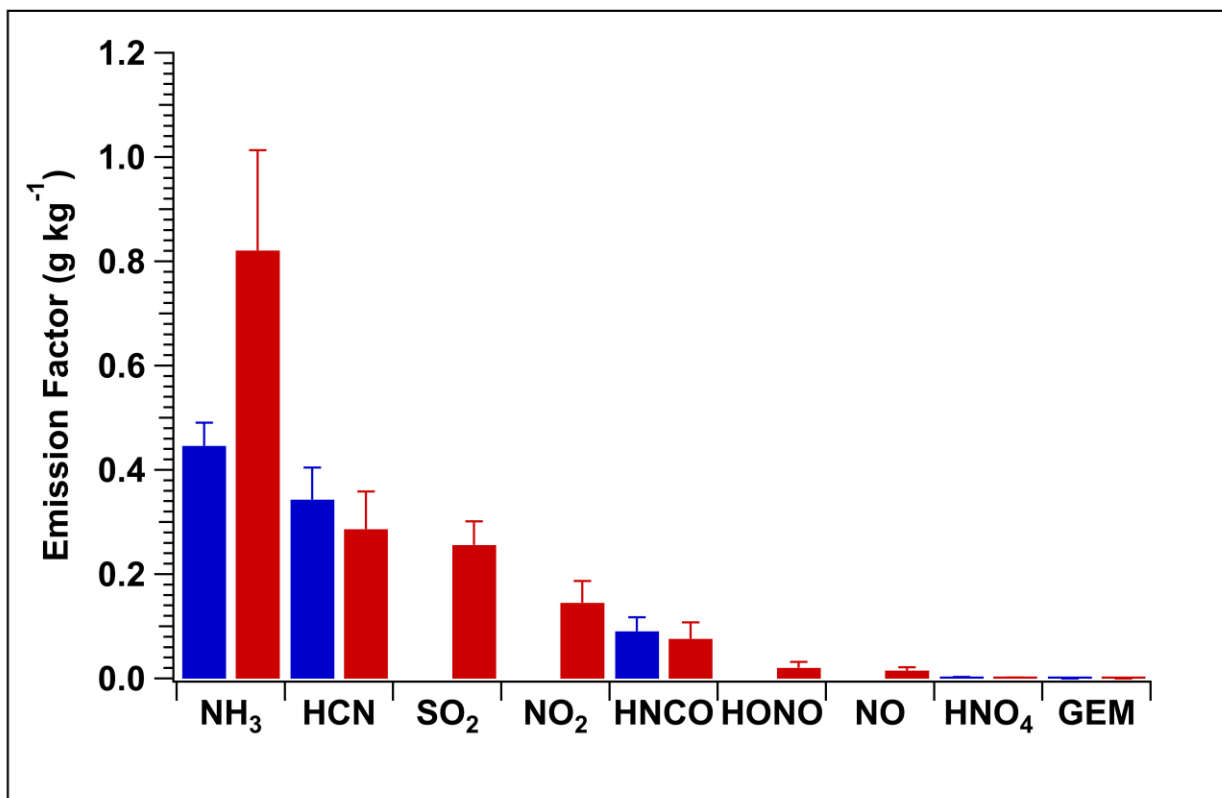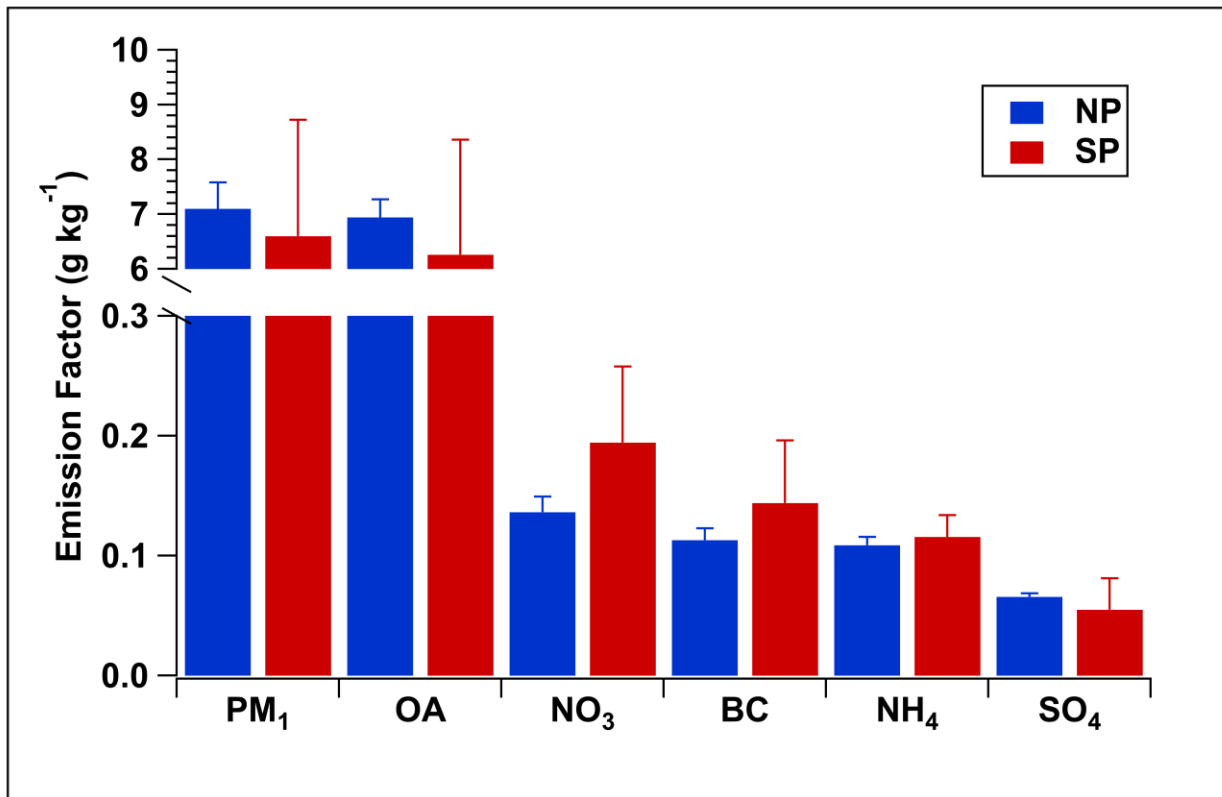
Figure S11. Emission factors (EF) (g kg^{-1}) for the SP and NP determined from measurements of a)
particle species; and b) inorganic gas-phase species.
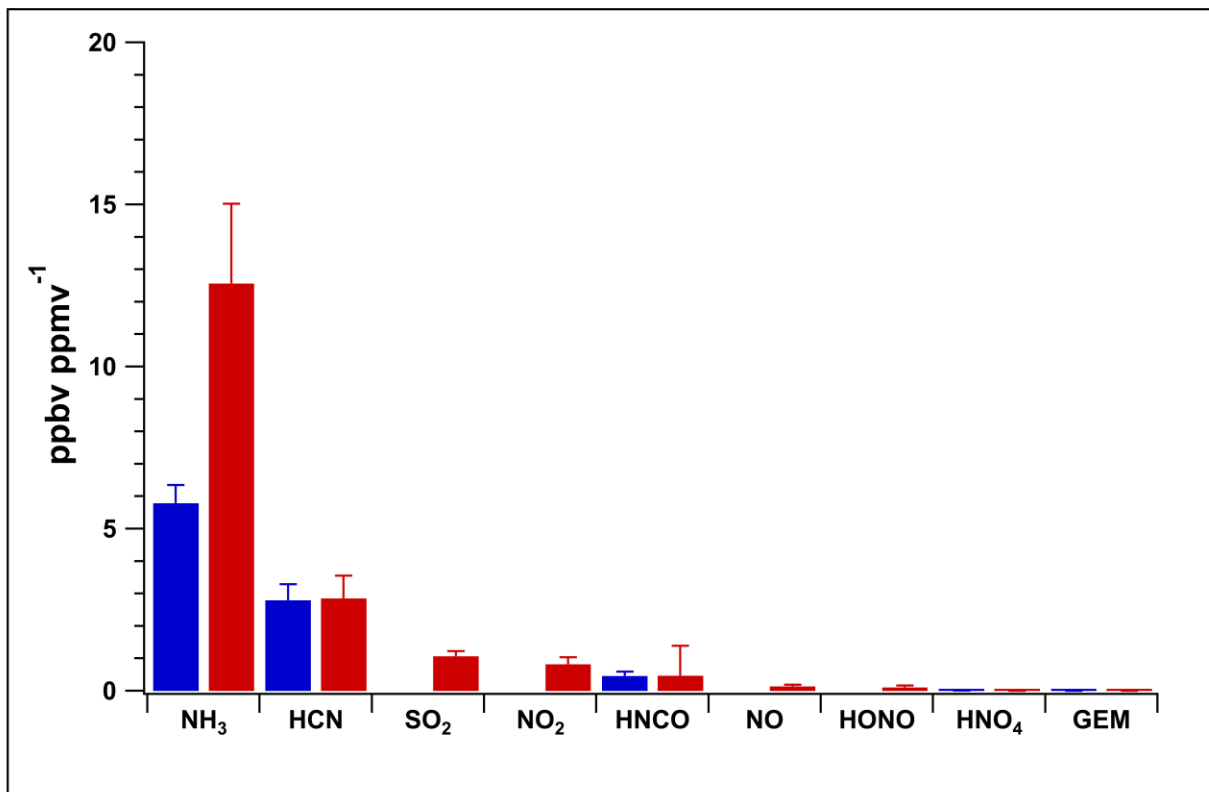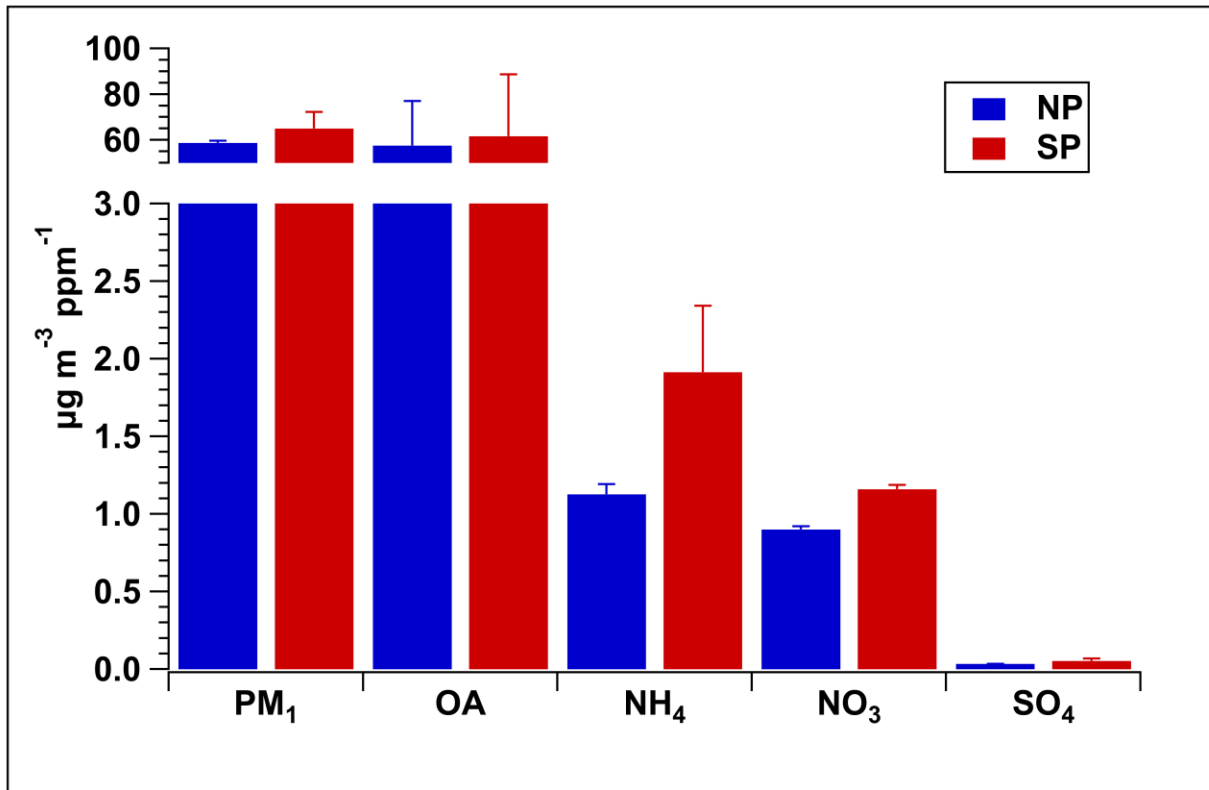
Figure S12. Emission ratios (ER) for the SP and NP determined from measurements of a) particle species (μg m^{-3} ppm^{-1}); and b) inorganic gas-phase species (ppb ppm^{-1}).

523

Figure S13. Emission factors (EF) (g kg^{-1}) for the a) NP and b) SP for the top 25 measured gas-phase
organic species. C4 acids = C4 oxo-carboxylic acids, propadiene = fragments/propadiene, hydroxy
acetone = hydroxy acetone/ ethyl formate; MEK = MEK, butanal and 2-methylpropanal .

528
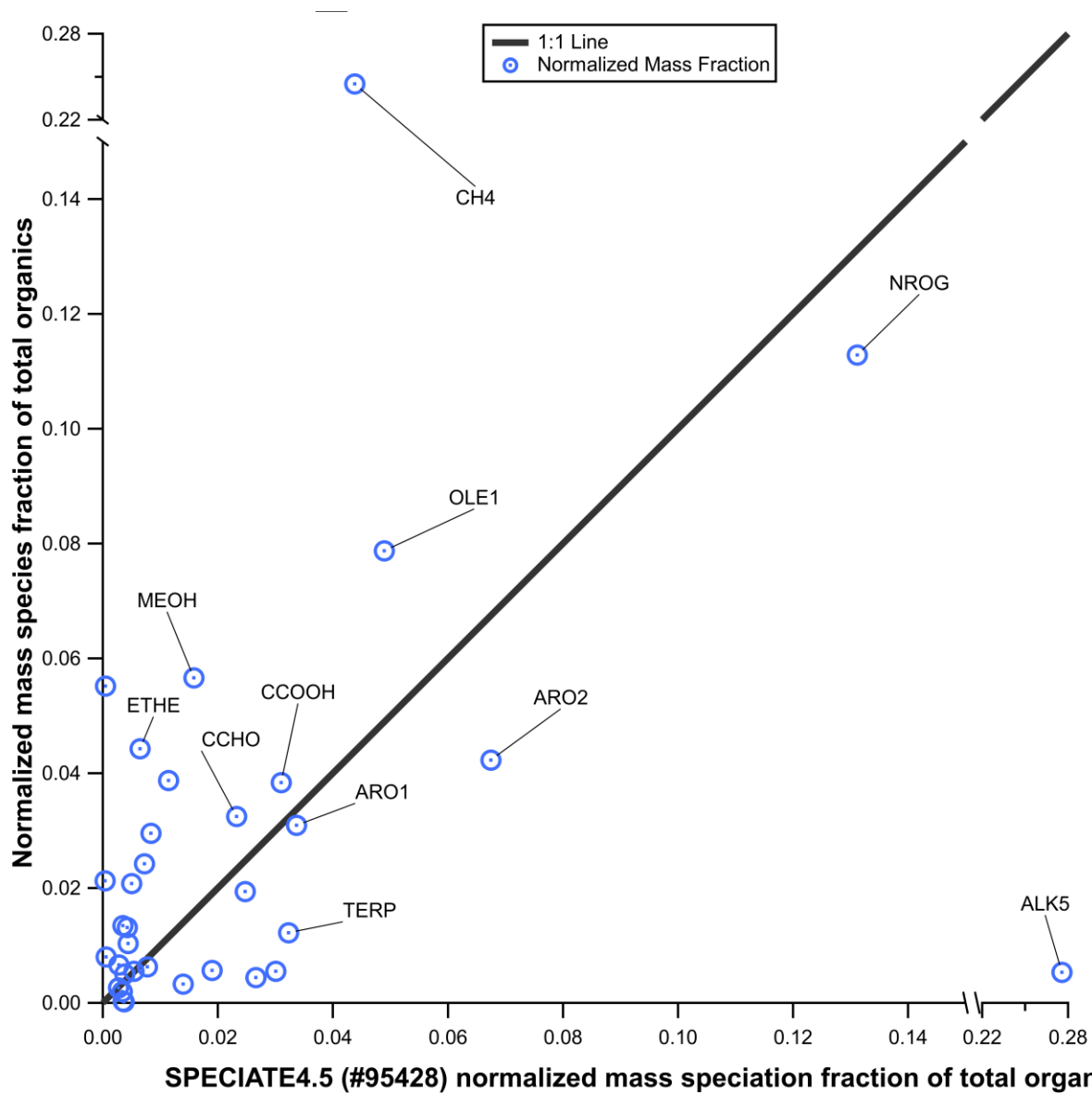
529   Figure S14. Comparison of the normalized organic gas speciation profile derived from this study with
530   that from the EPA's SPECIATE4.5 (#95428) profile.   EFs in the present study were mapped to the
531   SAPRC-11 model mechanism species and normalized to total organic gas (which does not include the
532   unidentified mass fraction), to create a total organic gas mass speciation profile. The total organic mass
533   speciation profile is plotted against the similarly treated mass speciation profile from the EPA
534   SPECIATEv4.5 #95428 for wildfire smoldering emissions. Note that for comparison purposes the non-
535   standard SAPRC-11 species in the present study are lumped, such that SESQ is summed with TERP, and
536   IVOC, WSOC and NVOL are summed with NROG.

537

538

539

540

43

References

Akagi, S. K., Yokelson, R. J., Wiedinmyer, C., Alvarado, M. J., Reid, J. S., Karl, T., Crounse, J. D., and Wennberg, P. O.: Emission factors for open and domestic biomass burning for use in atmospheric models, Atmos. Chem. Phys., 11, 4039-4072, https://doi.org/10.5194/acp-11-4039-2011, 2011.

Allan, J. D., Jimenez, J. L., Williams, P. I., Alfarra, M. R., Bower, K. N., Jayne, J. T., Coe, H., and Worsnop, D. R.: Quantitative sampling using an Aerodyne Aerosol Mass Spectrometer 1. Techniques of data interpretation and error analysis, J. Geophys. Res.-Atmos, 108, 4090, https://doi.org/10.1029/2002JD002358, 2003.

Andreae, M. O. and Merlet, P.: Emission of trace gases and aerosols from biomass burning, Global Biogeochem. Cy., 15, 955-966, https://doi.org/10.1029/2000GB001382, 2001.

Andreae, M. O.: Emission of trace gases and aerosols from biomass burning – an updated assessment, Atmos. Chem. Phys., 19, 8523-8546, https://doi.org/10.5194/acp-19-8523-2019, 2019. Biomass burning emission factors https://edmond.mpdl.mpg.de/imeji/collection/op2vVE8m0us_gcGC, ver 14 Apr 2021.

Baray, S., Darlington, A., Gordon, M., Hayden, K. L., Leithead, A., Li, S. M., Liu, P. S. K., Mittermeier, R. L., Moussa, S. G., O'Brien, J., Staebler, R., Wolde, M., Worthy, D., and McLaren, R.: Quantification of methane sources in the Athabasca Oil Sands Region of Alberta by aircraft mass balance, Atmos. Chem. Phys., 18, 7361-7378, https://doi.org/10.5194/acp-18-7361-2018, 2018.

Baumgardner, D., Kok, G., and Raga, G.: Warming of the Arctic lower stratosphere by light absorbing particles, Geophys. Res. Lett., 31, L06117, https://doi.org/10.1029/2003GL018883, 2004.

Bertschi, I., Yokelson, R. J., Ward, D. E., Babbitt, R. E., Susott, R. A., Goode, J. G., and Hao, W. M.: Trace gas and particle emissions from fires in large diameter and belowground biomass fuels, J. Geophys. Res.-Atmos, 108, 8472, https://doi.org/10.1029/2002JD002100, 2003.

Cai, Y., Montague, D. C., Mooiweer-Bryan, W., and Deshler, T.: Performance characteristics of the ultra high sensitivity aerosol spectrometer for particles between 55 and 800nm: Laboratory and field studies, J. Aerosol Sci., 39, 759-769, https://doi.org/10.1016/j.jaerosci.2008.04.007, 2008.

Clyne, M. A. A., Thrush, B. A., and Wayne, R. P.: Kinetics of the chemiluminescent reaction between nitric oxide and ozone, Trans. Faraday Soc., 60, 359-370, https://doi.org/10.1039/TF9646000359, 1964.

Cole, A. S., Steffen, A., Eckley, C. S., Narayan, J., Pilote, M., Tordon, R., Graydon, J. A., St. Louis, V. L., Xu, X., and Branfireun, B. A.: A survey of mercury in air and precipitation across Canada: Patterns and trends, Atmosphere, 5, 635-668, https://doi.org/10.3390/atmos5030635, 2014.

DeCarlo, P. F., Dunlea, E. J., Kimmel, J. R., Aiken, A. C., Sueper, D., Crounse, J., Wennberg, P. O., Emmons, L., Shinozuka, Y., Clarke, A., Zhou, J., Tomlinson, J., Collins, D. R., Knapp, D., Weinheimer, A. J., Montzka, D. D., Campos, T., and Jimenez, J. L.: Fast airborne aerosol size and chemistry measurements above Mexico City and Central Mexico during the MILAGRO campaign, Atmos. Chem. Phys., 8, 4027-4048, https://doi.org/10.5194/acp-8-4027-2008, 2008.

Ditto, J. C., He, M., Hass-Mitchell, T. N., Moussa, S. G., Hayden, K., Li, S. M., Liggio, J., Leithead, A., Lee, P., Wheeler, M. J., Wentzell, J. J. B., and Gentner, D. R.: Atmospheric evolution of emissions from a boreal forest fire: the formation of highly functionalized oxygen-, nitrogen-, and sulfur-containing organic compounds, Atmos. Chem. Phys., 21, 255-267, https://doi.org/10.5194/acp-21-255-2021, 2021.

Drewnick, F., Schwab, J. J., Jayne, J. T., Canagaratna, M., Worsnop, D. R., and Demerjian, K. L.: Measurement of ambient aerosol composition during the PMTACS-NY 2001 using an aerosol mass spectrometer. Part I: Mass concentrations special issue of aerosol science and technology on findings from the Fine Particulate Matter Supersites Program, Aerosol Sci. Tech., 38, 92-103, https://doi.org/10.1080/02786820390229507, 2004.

Dunlea, E. J., DeCarlo, P. F., Aiken, A. C., Kimmel, J. R., Peltier, R. E., Weber, R. J., Tomlinson, J., Collins, D. R., Shinozuka, Y., McNaughton, C. S., Howell, S. G., Clarke, A. D., Emmons, L. K., Apel, E. C., Pfister, G. G., van Donkelaar, A., Martin, R. V., Millet, D. B., Heald, C. L., and Jimenez, J. L.: Evolution of Asian aerosols during transpacific transport in INTEX-B, Atmos. Chem. Phys., 9, 7257-7287, https://doi.org/10.5194/acp-9-7257-2009, 2009.

Fehsenfeld, F. C., Dickerson, R. R., Hübler, G., Luke, W. T., Nunnermacker, L. J., Williams, E. J., Roberts, J. M., Calvert, J. G., Curran, C. M., Delany, A. C., Eubank, C. S., Fahey, D. W., Fried, A., Gandrud, B. W., Langford, A. O., Murphy, P. C., Norton, R. B., Pickering, K. E., and Ridley, B. A.: A ground-based intercomparison of NO, NO_x, and NO_y measurement techniques, J. Geophys. Res.-Atmos, 92, 14710-14722, https://doi.org/10.1029/JD092iD12p14710, 1987.

Gordon, M., Li, S. M., Staebler, R., Darlington, A., Hayden, K., O'Brien, J., and Wolde, M.: Determining air pollutant emission rates based on mass balance using airborne measurement data over the Alberta oil sands operations, Atmos. Meas. Tech., 8, 3745-3765, https://doi.org/10.5194/amt-8-3745-2015, 2015.
Hatch, L. E., Yokelson, R. J., Stockwell, C. E., Veres, P. R., Simpson, I. J., Blake, D. R., Orlando, J. J., and Barsanti, K. C.: Multi-instrument comparison and compilation of non-methane organic gas emissions from biomass burning and implications for smoke-derived secondary organic aerosol precursors, Atmos. Chem. Phys., 17, 1471-1489, https://doi.org/10.5194/acp-17-1471-2017, 2017.

Hayden, K.L., Li, S.M. Makar, P., Liggio, J., Moussa, S.G., Akingunola, A., McLaren, R., Staebler, R.M., Darlington, A. , O'Brien, J., Zhang, J., Wolde, M., and Zhang, L.: New methodology shows short atmospheric lifetimes of oxidized sulfur and nitrogen due to dry deposition, Atmos. Chem. Phys., 21, 8377–8392, https://doi.org/10.5194/acp-21-8377-2021, 2021.

Jimenez, J. L., Jayne, J. T., Shi, Q., Kolb, C. E., Worsnop, D. R., Yourshaw, I., Seinfeld, J. H., Flagan, R. C., Zhang, X., Smith, K. A., Morris, J. W., and Davidovits, P.: Ambient aerosol sampling using the Aerodyne Aerosol Mass Spectrometer, J. Geophys. Res.-Atmos, 108, 8425, https://doi.org/10.1029/2001JD001213, 2003.

Khare, P., Marcotte, A., Sheu, R., Walsh, A. N., Ditto, J. C., and Gentner, D. R.: Advances in offline approaches for trace measurements of complex organic compound mixtures via soft ionization and high-resolution tandem mass spectrometry, J. Chromatogr. A, 1598, 163-174, https://doi.org/10.1016/j.chroma.2019.03.037, 2019.

Kleinman, L. I., Springston, S. R., Daum, P. H., Lee, Y. N., Nunnermacker, L. J., Senum, G. I., Wang, J., Weinstein-Lloyd, J., Alexander, M. L., Hubbe, J., Ortega, J., Canagaratna, M. R., and Jayne, J.: The time evolution of aerosol composition over the Mexico City plateau, Atmos. Chem. Phys., 8, 1559-1575, https://doi.org/10.5194/acp-8-1559-2008, 2008.

Koss, A. R., Sekimoto, K., Gilman, J. B., Selimovic, V., Coggon, M. M., Zarzana, K. J., Yuan, B., Lerner, B. M., Brown, S. S., Jimenez, J. L., Krechmer, J., Roberts, J. M., Warneke, C., Yokelson, R. J., and de Gouw, J.: Non-methane organic gas emissions from biomass burning: identification, quantification, and emission factors from PTR-ToF during the FIREX 2016 laboratory experiment, Atmos. Chem. Phys., 18, 3299-3319, https://doi.org/10.5194/acp-18-3299-2018, 2018.

Kupc, A., Williamson, C., Wagner, N. L., Richardson, M., and Brock, C. A.: Modification, calibration, and performance of the Ultra-High Sensitivity Aerosol Spectrometer for particle size distribution and volatility measurements during the Atmospheric Tomography Mission (ATom) airborne campaign, Atmos. Meas. Tech., 11, 369-383, https://doi.org/10.5194/amt-11-369-2018, 2018.

Lee, B. H., Lopez-Hilfiker, F. D., Mohr, C., Kurtén, T., Worsnop, D. R., and Thornton, J. A.: An Iodide-Adduct High-Resolution Time-of-Flight Chemical-Ionization Mass Spectrometer: Application to Atmospheric Inorganic and Organic Compounds, Environmental Science & Technology, 48, 6309-6317, 10.1021/es500362a, 2014.

Lee, B. H., Lopez-Hilfiker, F. D., Veres, P. R., McDuffie, E. E., Fibiger, D. L., Sparks, T. L., Ebben, C. J., Green, J. R., Schroder, J. C., Campuzano-Jost, P., Iyer, S., D'Ambro, E. L., Schobesberger, S., Brown, S. S., Wooldridge, P. J., Cohen, R. C., Fiddler, M. N., Bililign, S., Jimenez, J. L., Kurtén, T., Weinheimer, A. J., Jaegle, L., and Thornton, J. A.: Flight Deployment of a High-Resolution Time-of-Flight Chemical Ionization Mass Spectrometer: Observations of Reactive Halogen and Nitrogen Oxide Species, Journal of Geophysical Research: Atmospheres, 123, 7670-7686, https://doi.org/10.1029/2017JD028082, 2018.

Leifer, I., Melton, C. Tratt, D.M., Buckland, K.N., Clarisse, L., Coheur, P., Frash, J., Gupta, M., Johnson, P.D., Leen, J.B., Van Damme, M., Whitburn, S., and Yurganov, L.: Remote sensing and in situ measurements of methane and ammonia emissions from a megacity dairy complex: Chino, CA, Environ. Poll., 221, 37-51, https://doi.org/10.1016/j.envpol.2016.09.083, 2017.

Lerner, B. M., Gilman, J. B., Aikin, K. C., Atlas, E. L., Goldan, P. D., Graus, M., Hendershot, R., Isaacman-VanWertz, G. A., Koss, A., Kuster, W. C., Lueb, R. A., McLaughlin, R. J., Peischl, J., Sueper, D., Ryerson, T. B., Tokarek, T. W., Warneke, C., Yuan, B., and de Gouw, J. A.: An improved, automated whole air sampler and gas chromatography mass spectrometry analysis system for volatile organic compounds in the atmosphere, Atmos. Meas. Tech., 10, 291-313, https://doi.org/10.5194/amt-10-291-2017, 2017.

Li, S.-M., Leithead, A., Moussa, S. G., Liggio, J., Moran, M. D., Wang, D., Hayden, K., Darlington, A., Gordon, M., Staebler, R., Makar, P. A., Stroud, C. A., McLaren, R., Liu, P. S. K., O'Brien, J., Mittermeier, R. L., Zhang, J., Marson, G., Cober, S. G., Wolde, M., and Wentzell, J. J. B.: Differences between measured and reported volatile organic compound emissions from oil sands facilities in Alberta, Canada, P. Natl. Acad. Sci. USA, 114, E3756-E3765, https://doi.org/10.1073/pnas.1617862114, 2017.

Li, K., Liggio, J., Han, C., Liu, Q., Moussa, S. G., Lee, P., and Li, S.-M.: Understanding the impact of high-NOx conditions on the formation of secondary organic aerosol in the photooxidation of oil sand-related precursors, Environ. Sci. Technol., 53, 14420-14429, https://doi.org/10.1021/acs.est.9b05404, 2019.

Li, K., Wentzell, J. J. B., Liu, Q., Leithead, A., Moussa, S. G., Wheeler, M. J., Han, C., Lee, P., Li, S.-M., and Liggio, J.: Evolution of atmospheric total organic carbon from petrochemical mixtures, Environ. Sci. Technol., 55, 12841-12851, https://doi.org/10.1021/acs.est.1c02620, 2021.

Liggio, J., Stroud, C. A., Wentzell, J. J. B., Zhang, J., Sommers, J., Darlington, A., Liu, P. S. K., Moussa, S. G., Leithead, A., Hayden, K., Mittermeier, R. L., Staebler, R., Wolde, M., and Li, S.-M.: Quantifying the Primary Emissions and Photochemical Formation of Isocyanic Acid Downwind of Oil Sands Operations, Environmental Science & Technology, 51, 14462-14471, 10.1021/acs.est.7b04346, 2017.

McGee, T.K.: Evacuating First Nations during wildfires in Canada, Fire Safety Journ., 120, https://doi.org/10.1016/j.firesaf.2020.103120, 2020.

McLagan, D. S., Stupple, G. W., Darlington, A., Hayden, K., and Steffen, A.: Where there is smoke there is mercury: Assessing boreal forest fire mercury emissions using aircraft and highlighting uncertainties associated with upscaling emissions estimates, Atmos. Chem. Phys., 21, 5635-5653, https://doi.org/10.5194/acp-21-5635-2021, 2021.

Middlebrook, A. M., Bahreini, R., Jimenez, J. L., and Canagaratna, M. R.: Evaluation of composition-dependent collection efficiencies for the aerodyne aerosol mass spectrometer using field data, Aerosol Sci. Tech., 46, 258-271, https://doi.org/10.1080/02786826.2011.620041, 2012.

Mungall, E. L., Abbatt, J. P. D., Wentzell, J. J. B., Lee, A. K. Y., Thomas, J. L., Blais, M., Gosselin, M., Miller, L. A., Papakyriakou, T., Willis, M. D., and Liggio, J.: Microlayer source of oxygenated volatile organic compounds in the summertime marine Arctic boundary layer, Proceedings of the National Academy of Sciences of the United States of America, 114, 6203-6208, 10.1073/pnas.1620571114, 2017.

Neuman, J. A., Huey, L. G., Ryerson, T. B., and Fahey, D. W.: Study of Inlet Materials for Sampling Atmospheric Nitric Acid, Environmental Science & Technology, 33, 1133-1136, 10.1021/es980767f, 1999.

Penkett, S., Gilge, S., Plass-Duelmer, C., Galbally, I., Brough, N., Bottenheim, J., Flocke, F., Gerwig, H., Lee, J., Milton, M., Rohrer, F., Ryerson, T., Steinbacher, M., Torseth, K., and Wielgosz, R.: WMO/GAW expert workshop on global long-term measurements of nitrogen oxides and recommendations for GAW nitrogen oxides network, World Meteorological Organization, Hohenpeissenberg, Germany, 2011.

Permar, W., Wang, Q., Selimovic, V., Wielgasz, C., Yokelson, R. J., Hornbrook, R. S., Hills, A. J., Apel, E. C., Ku, I.-T., Zhou, Y., Sive, B. C., Sullivan, A. P., Collett Jr, J. L., Campos, T. L., Palm, B. B., Peng, Q., Thornton, J. A., Garofalo, L. A., Farmer, D. K., Kreidenweis, S. M., Levin, E. J. T., DeMott, P. J., Flocke, F., Fischer, E. V., and Hu, L.: Emissions of trace organic gases from western U.S. wildfires based on WE-CAN aircraft measurements, J. Geophys. Res.-Atmos, 126, e2020JD033838, https://doi.org/10.1029/2020JD033838, 2021.

Quinn, P. K., Bates, T. S., Coffman, D., Onasch, T. B., Worsnop, D., Baynard, T., de Gouw, J. A., Goldan, P. D., Kuster, W. C., Williams, E., Roberts, J. M., Lerner, B., Stohl, A., Pettersson, A., and Lovejoy, E. R.: Impacts of sources and aging on submicrometer aerosol properties in the marine boundary layer across the Gulf of Maine, J. Geophys. Res.-Atmos, 111, D23S36, https://doi.org/10.1029/2006JD007582, 2006.

Reid, J. S., and Hobbs, P. V.: Physical and optical properties of young smoke from individual biomass fires in Brazil, J. Geophys. Res.-Atmos., 103, 32013-32030, 10.1029/98jd00159, 1998.

Reid, J. S., Koppmann, R., Eck, T. F., and Eleuterio, D. P.: A review of biomass burning emissions part II: intensive physical properties of biomass burning particles, Atmos. Chem. Phys., 5, 799-825, 10.5194/acp-5-799-2005, 2005.

Ridley, B. A. and Grahek, F. E.: A small, low flow, high sensitivity reaction vessel for NO chemiluminescence detectors, J. Atmos. Ocean. Tech., 7, 307-311, https://doi.org/10.1175/1520-0426(1990)007<0307:Aslfhs>2.0.Co;2, 1990.

Roberts, J. M., Veres, P., Warneke, C., Neuman, J. A., Washenfelder, R. A., Brown, S. S., Baasandorj, M., Burkholder, J. B., Burling, I. R., Johnson, T. J., Yokelson, R. J., and De Gouw, J.: Measurement of HONO, HNCO, and other inorganic acids by negative-ion proton-transfer chemical-ionization mass spectrometry (NI-PT-CIMS): Application to biomass burning emissions, Atmospheric Measurement Techniques, 3, 981-990, 10.5194/amt-3-981-2010.

709 Schwarz, J. P., Gao, R. S., Fahey, D. W., Thomson, D. S., Watts, L. A., Wilson, J. C., Reeves, J. M.,
710 Darbeheshti, M., Baumgardner, D. G., Kok, G. L., Chung, S. H., Schulz, M., Hendricks, J., Lauer, A.,
711 Kärcher, B., Slowik, J. G., Rosenlof, K. H., Thompson, T. L., Langford, A. O., Loewenstein, M., and
712 Aikin, K. C.: Single-particle measurements of midlatitude black carbon and light-scattering aerosols from
713 the boundary layer to the lower stratosphere, J. Geophys. Res.-Atmos, 111, D16207,
714 https://doi.org/10.1029/2006JD007076, 2006.

715 Sekimoto, K., Li, S.-M., Yuan, B., Koss, A., Coggon, M., Warneke, C., and de Gouw, J.: Calculation of
716 the sensitivity of proton-transfer-reaction mass spectrometry (PTR-MS) for organic trace gases using
717 molecular properties, Int. J. Mass Spectrom., 421, 71-94, https://doi.org/10.1016/j.ijms.2017.04.006,
718 2017.

719 Selimovic, V., Yokelson, R. J., McMeeking, G. R., and Coefield, S.: In situ measurements of trace gases,
720 PM, and aerosol optical properties during the 2017 NW US wildfire smoke event, Atmos. Chem. Phys.,
721 19, 3905-3926, https://doi.org/10.5194/acp-19-3905-2019, 2019.

722 Sheu, R., Marcotte, A., Khare, P., Charan, S., Ditto, J. C., and Gentner, D. R.: Advances in offline
723 approaches for chemically speciated measurements of trace gas-phase organic compounds via adsorbent
724 tubes in an integrated sampling-to-analysis system, J. Chromatogr. A, 1575, 80-
725 90, https://doi.org/10.1016/j.chroma.2018.09.014, 2018.

726 Stecher III, H. A., Luther III, G. W., MacTaggart, D. L., Farwell, S. O., Crosley, D. R., Dorko, W. D.,
727 Goldan, P. D., Beltz, N., Krischke, U., Luke, W. T., Thornton, D. C., Talbot, R. W., Lefer, B. L., Scheuer,
728 E. M., Benner, R. L., Wu, J., Saltzman, E. S., Gallagher, M. S., and Ferek, R. J.: Results of the Gas-Phase
729 Sulfur Intercomparison Experiment (GASIE): Overview of experimental setup, results and general
730 conclusions, J. Geophys. Res.-Atmos, 102, 16219-16236, https://doi.org/10.1029/97JD01362, 1997.

731 Stephens, M., Turner, N., and Sandberg, J.: Particle identification by laser-induced incandescence in a
732 solid-state laser cavity, Appl. Optics, 42, 3726-3736, https://doi.org/10.1364/ao.42.003726, 2003.

733 Stockwell, C. E., Kupc, A., Witkowski, B., Talukdar, R. K., Liu, Y., Selimovic, V., Zarzana, K. J.,
734 Sekimoto, K., Warneke, C., Washenfelder, R. A., Yokelson, R. J., Middlebrook, A. M., and Roberts, J.
735 M.: Characterization of a catalyst-based conversion technique to measure total particulate nitrogen and
736 organic carbon and comparison to a particle mass measurement instrument, Atmos. Meas. Tech., 11,
737 2749-2768, 10.5194/amt-11-2749-2018, 2018.

738 Veres, P. R., and Roberts, J. M.: Development of a photochemical source for the production and
739 calibration of acyl peroxynitrate compounds, Atmos. Meas. Tech., 8, 2225-2231, 10.5194/amt-8-2225-
740 2015, 2015.

741 Veres, P., Roberts, J. M., Burling, I. R., Warneke, C., de Gouw, J., and Yokelson, R. J.: Measurements of
742 gas-phase inorganic and organic acids from biomass fires by negative-ion proton-transfer chemical-
743 ionization mass spectrometry, J. Geophys. Res.-Atmos, 115, D23302,
744 https://doi.org/10.1029/2010JD014033, 2010.

745 Ward, D. E. and Radke, L. F.: Emissions measurements from vegetation fires: A comparative evaluation
746 of methods and results, in: Fire in the Environment: The Ecological, Atmospheric, and Climatic
747 Importance of Vegetation Fires. Dahlem Workshop Reports: Environmental Sciences Research Report
748 13, edited by: Crutzen, P. J., and Goldammer, J. G., John Wiley & Sons, Chischester, England, 53-76,
749 1993.

750   Williams, E. J., Baumann, K., Roberts, J. M., Bertman, S. B., Norton, R. B., Fehsenfeld, F. C.,

751   Springston, S. R., Nunnermacker, L. J., Newman, L., Olszyna, K., Meagher, J., Hartsell, B., Edgerton, E.,

752   Pearson, J. R., and Rodgers, M. O.: Intercomparison of ground-based NO_y measurement techniques, J.

753   Geophys. Res.-Atmos, 103, 22261-22280, https://doi.org/10.1029/98JD00074, 1998.

754

755

756

757